Evaluating the Consistency and Continuity of Pixel-Scale Cloud Property Data Records From *Aqua* and *SNPP*

Qing Yue[1], Eric J. Fetzer[1], Likun Wang[2], Brian H. Kahn[1], Nadia Smith[3], John Blaisdell[4], Kerry G. Meyer[5], Mathias Schreier[1], Bjorn Lambrigtsen[1], and Irina Tkatcheva[1]

[1]Jet Propulsion Laboratory, California Institute of Technology, Pasadena, CA
[2] Earth System Science Interdisciplinary Center, University of Maryland, 5825 University Research Court, Suite 4001, College Park, MD 20740.
[3]Science and Technology Corporation, 10015 Old Columbia Road, Columbia, MD 21046 [4]Science Applications International Corporation, 12010 Sunset Hills Road, Reston, VA 20190 [5]NASA Goddard Space Flight Center, Greenbelt, MD.

© 2022. All rights reserved.

Correspondence to: Qing Yue (qing.yue@jpl.nasa.gov)

Abstract

The *Aqua*, *SNPP*, and *JPSS* satellites carry a combination of hyperspectral infrared sounders (AIRS, CrIS) and high-spatial-resolution narrowband imagers (MODIS, VIIRS). They provide an opportunity to acquire high-quality long-term cloud data records and are a key component of the existing Program of Record of cloud observations. By matching observations from sounders and imagers across different platforms at pixel scale, this study evaluates the self-consistency and continuity of cloud retrievals from *Aqua* and *SNPP* by multiple algorithms, including the AIRS Version-7 retrieval algorithm and the Community Long-term Infrared Microwave Combined Atmospheric Product System (CLIMCAPS) Version-2 for sounders, and the Standard *Aqua*MODIS Collection-6.1 and the NASA MODIS-VIIRS continuity cloud products for imagers. Metrics describing detailed statistical distributions at sounder field of view (FOV) and the joint histograms of cloud properties are evaluated. These products are found highly consistent despite their retrieval from different sensors using different algorithms. Differences between the two sounder cloud products are mainly due to cloud clearing and treatment of clouds in scenes with unsuccessful atmospheric profile retrievals. The sounder subpixel cloud heterogeneity evaluated using the standard deviation of imager retrievals at sounder FOV shows good agreement between the standard and continuity products from different satellites. However, impact of algorithm and instrument differences between MODIS and VIIRS is revealed in cloud top pressure retrievals and in the imager cloud distribution skewness. Our study presents a unique aspect to examine NASA's progress toward building a continuous cloud data record with sufficient quality to investigate clouds' role in global environmental change.

1. Introduction

Clouds play an important role in Earth's energy balance and hydrological cycle. They occur with processes involving atmospheric radiation, thermodynamics, and dynamics at various spatial and temporal scales, making clouds a crucial component of the weather and climate system. With daily regional and global coverage, space observations provide a unique vantage point to monitor the change of the cloud properties in the climate system across different time scales. This offers an important observational basis to resolve cloud processes in the background atmospheric circulation, which is widely recognized as a critical challenge within Earth Sciences (Bony et al. 2015, IPCC 2013). The 2017 US National Academy Decadal Survey (ESAS 2017) has noted the importance of long-term and sustained observations of many key components of the Earth system, including continuity measurements of clouds. Many of these observations are obtained from the existing Program of Record (POR). Since the "POR forms the foundation upon which the committee's recommendations are established" (ESAS 2017), it is crucial to evaluate whether a self-consistent and continuous POR for cloud-related variables is indeed available with sufficient data quality and spatio-temporal coverage.

Cloud retrievals from the NASA's Earth Observing System (EOS) satellites, including *Terra* and *Aqua*, the joint NASA/NOAA Suomi National Polar-orbiting Partnership (*SNPP*), and NOAA's new generation of Joint Polar Satellite System (*JPSS*) series weather satellites, are a key component in the POR for cloud properties. Through efforts on continuity and consistency by rigorous instrument mission design and ongoing algorithm development, these satellites provide high quality, long-term cloud data records derived from the Top of Atmosphere (TOA) radiances observed across a wide range of the emission and reflection spectrum. Particularly, *Aqua*, *SNPP*,

and *JPSS-1* (now *NOAA-20*), which were launched in 2002, 2011, and 2016, respectively, carry high spatial resolution narrowband imagers, hyperspectral infrared (IR) sounders, and microwave (MW) sounding measurements. As a result, observations with similar spatial resolution and coverage, and similar spectral resolution at analogous wavelengths are obtained from different satellites. For *Aqua*, this instrument trio consists of the Atmospheric Infrared Sounder (AIRS), the Advanced Microwave Sounding Unit (AMSU), and the Moderate Resolution Imaging Spectroradiometer (MODIS). For *SNPP* and *JPSS*, the trio includes the Cross-track Infrared Sounder (CrIS), the Advanced Technology Microwave Sounder (ATMS), and the Visible Infrared Imaging Radiometer Suite (VIIRS).

Retrieval algorithms to maintain the continuity of the data records across these platforms have been developed. For joint retrievals by IR and MW sounders such as AIRS/AMSU and CrIS/ATMS, the Community Long-term Infrared Microwave Combined Atmospheric Product System (CLIMCAPS; Smith and Barnet, 2019) provides cloud properties together with vertical profiles of atmospheric temperature, water vapor, and trace gases, as well as surface conditions. For imagers like MODIS and VIIRS, the NASA MODIS-VIIRS continuity cloud products have been developed for both cloud mask (CLDMSK; Frey et al. 2020) and cloud optical properties (CLDPROP; Platnick et al. 2021). These continuity algorithms have heritage with NASA operational retrieval products previously developed for individual sensors and satellites, such as the AIRS Science Team retrieval algorithm Version 7 (AIRS V7, Yue and Lambrigsten 2017, 2020) in the case of CLIMCAPS, and the Standard *Terra*/*Aqua* MODIS Collection 6.1 cloud retrievals (MOD35/MYD35, MOD06/MYD06; Baum et al. 2012, Platnick et al. 2017) in the case of MODIS-VIIRS. However, significant differences exist between the standard and continuity algorithms, as the focus of the continuity algorithms is to minimize the impact of instrument between platforms.

The sounder-imager combination on the same sun-synchronous polar-orbiting satellite, together with the temporal coverage overlap between satellites, provides opportunities to utilizing spectral and spatial capabilities from different sensors at global scale. Previous studies have shown the benefits of using the combined information to intercalibrate and test radiometric consistency among sensors (Tobin et al. 2006, Schreier et al. 2010, Wong et al. 2015, Gong et al. 2018); crossvalidate the retrievals (Nasiri et al. 2011, Kahn et al. 2014); further improve atmospheric and surface geophysical parameter retrievals (Irion et al. 2018, Yao et al. 2015); provide simultaneous observations to resolve complex physical processes (Yue et al. 2013, 2016, 2019, McCoy et al. 2017); quantify the subpixel heterogeneity (Li et al. 2004, Kahn et al. 2015); and enhance the utilization of satellite observations in numerical weather prediction and climate models (Eresmaa 2014). Therefore, the sounder-imager combination is an important aspect of data record continuity and consistency among sensors across different platforms. This helps provide robust monitoring of long-term changes in cloud properties, an important capability expected from the POR.

Pixel-scale analyses are an effective and unique way to investigate the consistency and continuity of these data records because of the one-to-one relationships established by these comparisons and their direct links to algorithm performance. This includes examining differences of (1) the same physical parameters observed by different sensors or satellites but processed using the same (or similar) algorithms, and (2) the same parameters obtained from the same sensor but from different algorithms. Both of these differences are quantified at the pixel scale in this study. The cloud properties determined by the sounder and imager pairs on board *Aqua* and *SNPP*, namely AIRS/MODIS and CrIS/VIIRS, are investigated using the collocated sounder-imager fields of view (FOVs) for sets of pixels obtained during Simultaneous Nadir Observations (SNOs) between *Aqua*-AIRS and *SNPP*-CrIS. This approach ensures nearly identical viewing geometry by the two

satellites while pixel-scale cloud assessment is carried out by comparing cloud parameters determined by hyperspectral IR sounders and high spatial resolution imagers at the minimum spatial scale of individual instrument fields of view. Using this approach, products from both the heritage NASA standard retrieval algorithms and the newly-developed continuity cloud algorithms are analyzed (Table 1). This is essential for retrieval algorithm development and crossvalidation of multiple sensors and products on *Aqua* and *SNPP*, and also important for data continuity extending to future *JPSS* satellites.

This article is organized as follows. Section 2 describes various cloud products and their retrieval algorithms analyzed in this study, as well as the method used to create pixel-scale collocated datasets between sounders and imagers across different satellites. Section 3 shows the detailed comparisons of cloud properties and their joint histograms from different algorithms and sensors, and the discussions on implications on retrieval algorithm development and instrument differences. A summary and set of conclusions are presented in Section 4.

2. Data and Methodology

2.1 Cloud products and algorithms

Table 1 summarizes the cloud parameters analyzed in this study from various Level 2 (L2) retrieval products derived from the sounders and imagers aboard *Aqua* and *SNPP*. For AIRS and MODIS, both the standard operational and continuity products are evaluated: the AIRS V7 and CLIMCAPS-*Aqua* Version 2 (V2) retrievals for AIRS, and the Collection 6.1 *Aqua* MODIS Atmosphere Level 2 Cloud Product (MYD06) and Version 1.1 NASA *Aqua* MODIS Continuity Cloud Property Products (CLDPROP_MODIS). For *SNPP*-CrIS and -VIIRS, only the continuity products are evaluated, which are the V2 CLIMCAPS-*SNPP* and Version 1.1 *SNPP*-VIIRS

129 Continuity Cloud Property Products (CLDPROP_VIIRS). The CLIMCAPS-*SNPP* products were
130 produced using Version 2 of the CrIS Level-1B product in Nominal Spectral Resolution (NSR)
131 and Full Spectral Resolution (FSR), which differ in the spectral resolution of the shortwave and
132 mid-IR CrIS observations transmitted from *SNPP* (Monarrez et al. 2020). The spectral resolution
133 differences cause subtle differences between the CLIMCAPS FSR and NSR retrievals, especially
134 in the upper tropospheric humidity and trace gases (Wang et al. 2021).

135 In both the AIRS V7 and CLIMCAPS algorithms for AIRS and CrIS, the radiatively effective
136 cloud amount (effective cloud fraction, ECF) and cloud top pressure (CTP) are retrieved by
137 matching the calculated cloudy radiances with the observed radiances for a set of channels that are
138 sensitive to clouds. Then the cloud top temperature (CTT) is derived as the atmospheric
139 temperature matching the retrieved CTP. In this process, best estimates of surface and atmospheric
140 parameters are used to calculate the cloudy radiances, either from the *a priori* state or from the
141 physical retrieval after the cloud clearing step (Susskind et al. 2003, Susskind et al. 2006, Smith
142 and Barnet 2019). The cloud clearing approach (Chahine 1974) is applied in both the AIRS Science
143 Team algorithms and CLIMCAPS. It predicts a single cloud cleared radiance at one AMSU or
144 ATMS field of regard (FOR) using *a priori* temperature, water vapor, and surface information and
145 a linear combination of IR radiances from nine AIRS or CrIS FOVs that are co-registered with one
146 AMSU or ATMS FOR (Susskind et al. 2003). The cloud cleared radiances are subsequently used
147 to retrieve surface and atmospheric parameters. Flowcharts of the retrieval steps and differences in
148 these two sounder retrieval systems are given in Thrastarson et al. (2021).

149 The ECF is the product of cloud areal fraction and the IR cloud emissivity, the latter of which
150 is assumed to be spectrally flat in the retrieval of ECF (Susskind et al. 2003). Previous studies show
151 that the AIRS ECF is consistent with the cloud properties such as the cloud frequency and cloud

optical depth measured by CloudSat and MODIS (Yue et al. 2011, Kahn et al. 2014). The AIRS and CrIS retrievals of ECF and cloud top properties (CTT and CTP) are reported for up to two cloud layers in each IR sounder FOV (~13.5 km spatial resolution at nadir).

There are distinct differences between the AIRS V7 and CLIMCAPS V2 algorithms regarding cloud retrievals, summarized here. The first major difference is how cloud clearing is iterated in the retrieval flow. The second major algorithm difference is quality control (QC) procedures when 1) the physical retrieval of atmosphere and surface is not successful, and 2) the final-stage cloud clearing is not successful (Susskind et al. 2014). The third major difference is the choice of the prior states for the two algorithms. The AIRS Science Team algorithms, including both V6 and V7, iterate cloud clearing multiple times, and cloud parameters are determined after the last iteration of cloud clearing using the retrieved surface and atmospheric conditions (Fetzer et al. 2020). In contrast, CLIMCAPS V2 performs a single cloud clearing pass and cloud properties are retrieved using the surface and atmospheric parameters from successful retrievals of surface and atmospheric properties (Smith and Barnet 2019, Thrastarson et al. 2021). The QC procedure used in the two sounder cloud retrievals are also different. AIRS V7 produces case-by-case QC indicators for each retrieved variable; while CLIMCAPS V2 derives one QC value based on the cloud clearing and retrieval status of temperature and water vapor, and the same QC value is assigned to all retrieved variables for the given FOV, including the cloud parameters. Particularly, in AIRS V7 cloud retrieval process, the final stage of cloud clearing and cloud retrievals uses the surface and atmospheric variable retrievals, except for cases over ocean when the retrieved surface temperature differs from the first guess by more than 5 K. For these cases, the surface temperature and surface emissivity from the *a priori* are used instead, and cloud properties retrieved under this condition are flagged as valid with QC=1, indicating successful cloud retrievals but potentially higher

uncertainty than QC=0. This surface test effectively filters out cases when the cloud top is misidentified as surface and causes extremely small ECF values for overcast cloudy conditions over ocean. For ~1% of cases the final cloud retrieval step does not complete successfully, and a QC=2 flag is assigned to cloud parameters to indicate invalid retrievals. As a result, the AIRS V7 cloud retrievals produce a much higher percentage of cases with successful cloud retrievals (cloud variable QC=0 or QC=1) than its temperature and water vapor profile products. For CLIMCAPS V2, cloud clearing is not iterated and cloud parameters follow the QC procedure in the physical atmospheric state retrievals. As a result, a much larger number of cases with QC=2 cloud retrievals are reported by CLIMCAPS V2 compared to AIRS V7, especially for cloudier conditions or cases with large cloud clearing errors, typically those FORs with low cloud contrast between associated FOVs. Different *a priori* in the two retrieval systems impact their cloud retrievals. AIRS V7 uses the Stochastic Cloud Clearing / Neural Network (SCCNN) solution as *a priori* on atmospheric temperature and water vapor profiles and surface temperature trained using a few months of AIRS/AMSU radiances and European Center for Medium-Range Weather Forecasting (ECMWF) Integrated Forecast System (IFS) 3-hourly forecast fields that are collocated to AIRS observations (including updates since Version CY31R1: https://www.ecmwf.int/en/forecasts/documentation-and-support/changes-ecmwf-model) (Milstein and Blackwell 2016). For land and sea ice surface emissivity prior estimates, AIRS V7 uses the University of Wisconsin – Madison Baseline Fit Emissivity database (Seemann et al. 2008), which is based on the monthly climatology of MODIS land surface emissivity product (MOD11) in 2008 (Thrastarson et al. 2021). The CLIMCAPS system (Smith and Barnet 2020, Smith et al. 2021), instead, uses concurrent fields from the Version 2 ModernEra Retrospective analysis for Research and Application (MERRA-2, Gelaro et al. 2017) as the *a priori* and implements the Combined ASTER (Advanced Spaceborne Thermal Emission

198 and Reflection Radiometer) and MODIS Emissivity database for land surface (Hook 2019, Borbas
199 et al., 2018, Feltz et al. 2018). Over ocean, both systems use the Masuda IR sea surface emissivity
200 model (Masuda et al., 1988) as modified by Wu and Smith (1997). Since the *a priori* temperature,
201 water vapor, and surface properties are used in the cloud clearing step, differences in the *a priori*
202 contribute to the differences between the retrieval products, including cloud properties (Yue and
203 Lambrigtsen 2020, Yue et al. 2021). Cloud clearing plays an important role in both retrieval
204 systems, and physical retrievals of surface and atmospheric parameters are obtained from the cloud
205 cleared radiances, which, in turn, impact the determination of cloud properties.
206 In addition to these major differences, the two sounder retrieval systems differ in the prior
207 estimates used for ECF and CTP. CLIMCAPS starts the cloud retrieval with background estimates
208 of 0.5 and 0.25 ECF at 350 hPa and 800 hPa CTP for the upper and lower cloud layers, respectively.
209 AIRS V7 uses 1/6 ECF at 350 hPa for the upper layer, and 1/3 ECF at 850 hPa (or 100 hPa above
210 surface in elevated terrain) for the lower cloud layer. However, since the final cloud retrievals of
211 both systems are shown to diverge significantly from their prior (Yue and Lambrigtsen 2020, Yue
212 et al. 2021), it is unlikely that different cloud prior estimates are a main contributor to the sounder
213 cloud retrieval product differences.
214 Although their spectral resolution is coarser than that of AIRS and CrIS, instruments like
215 MODIS and VIIRS provide high spatial-resolution cloud properties through information in
216 multiple narrowband channels covering the visible and IR spectral regions. However, significant
217 differences exist between the two imagers. MODIS measures the reflectance or radiance in 36
218 spectral bands, while VIIRS has an analogous subset of these bands (20 channels) plus a day/night
219 visible channel (Oudrari et al. 2015). The lack of near-IR and IR water vapor and CO_2 absorption
220 channels in VIIRS has important implications on the available information content for clouds with

respect to MODIS. This impacts the determination of clouds, especially the detection of multilayer clouds and clear sky in polar night conditions, and the determination of cloud thermodynamic phase. It also impacts the retrieval of cloud-top properties, especially for high thin clouds. Moreover, the difference of spectral location of the VIIRS 2.25 μm channel compared to the analogous 2.13 μm MODIS channel has implications on the retrievals of cloud particle size, optical depth, and thermodynamic phase (Platnick et al. 2020), which will be briefly summarized in the following discussions. On the other hand, VIIRS provides a higher spatial resolution of 750 m at nadir in cloud property retrievals, compared to the 1-km resolution in the Collection 6.1 MYD06 and cloud mask products. In addition, VIIRS has an onboard detector aggregation scheme that limits the across-swath pixel growth. VIIRS edge of scan pixel size is roughly 1.625 km x 1.625 km versus roughly 2km x 4.9 km for MODIS (Platnick et al. 2021). The MYD06 products have been shown to provide stable and well characterized cloud data records since 2002 (e.g. Yue et al. 2017). Given these instrument differences between MODIS and VIIRS, and a need to develop a continuous data record extending beyond the MODIS era, the MODISVIIRS CLDMSK cloud mask (Frey et al. 2020) and CLDPROP cloud-top and optical property (Platnick et al. 2021) continuity algorithms were developed. By applying common algorithms to a subset of channels available on both instruments, the continuity algorithms accommodate the detailed channel differences between the two instruments while maximizing the information content on cloud parameters.

The continuity CLDPROP products use only spectral channels common to both MODIS and VIIRS. The algorithm has direct heritage with the Collection 6.1 MODIS atmosphere cloud retrievals (MYD06), with cloud-top property datasets provided by the CLouds from AVHRR (the Advanced Very High Resolution Radiometer) - Extended (CLAVR-x) processing system

(Heidinger et al. 2012, 2014) to account for more limited information for cloud-top property retrieval. CLAVR-x produces cloud phase reported as Cloud_Phase_Cloud_Top_Properties in the MODIS-VIIRS continuity cloud products. Since VIIRS does not have IR channels in the 13 μm CO_2 absorption band, the MODIS CO_2 slicing solution for cloud top pressure retrievals for cold clouds is replaced with an IR window channel optimal estimation approach coupled with a Cloud-Aerosol Lidar and Infrared Pathfinder Satellite Observations (CALIPSO)-derived *a priori* (Heidinger et al. 2019). This in turn affects the optical property cloud phase algorithm (reported as Cloud_Phase_Optical_Properties in CLDPROP products), which removes the cold cloud sanity check applied in the MOD06/MYD06 that is based on the CO_2-slicing solution. The spectral mismatch of the MODIS 2.13 μm and VIIRS 2.25 μm channels also bring further changes to the Cloud_Phase_Optical_Properties retrieval by modifying the spectral cloud effective radius (Re) test approach. In the Version 1.1 MODIS-VIIRS continuity cloud product used in this study, the 2.25 μm test is omitted and the 1.61 μm test is duplicated. Moreover, this channel spectral differences compel changes in the look-up tables (LUT) of spectral liquid cloud reflectance used in the retrieval, which include the use of an updated liquid water imaginary index of refraction dataset in the shortwave infrared region (Kuo et al. 1993) and an updated complex index of refraction dataset for 3.7 μm (Wagner et al. 2005). Such differences in LUTs result in changes of cloud effective particle size (Re) (Platnick et al. (2020) that, along with cloud optical depth (COD), are used to derive cloud water path. Moreover, the ice crystal absorption at 2.25 μm is weaker than that at 2.13 μm. Differences with the Collection 6.1 MODIS cloud retrieval algorithms, as well as inter-sensor differences between MODIS and VIIRS, have been reported in detail in recent studies such as Frey et al. (2020) and Platnick et al. (2021), which are based on granule comparisons and long-term mean statistics.

2.2 Simultaneous Nadir Observations (SNOs) of collocated satellites

The pixel-scale comparisons will use SNOs between *Aqua*-AIRS and *SNPP*-CrIS. These SNOs contain pixel pairs of observations from the two instruments when they observe the same location at approximately the same scan angle and time. The AIRS-CrIS SNOs used herein were originally developed by the JPL Sounder Science Investigator Processing System (SIPS) for inter-calibration of two sounders (Manning and Aumann 2015). In order to ensure a close match between the instruments, the following criteria are used to identify candidate SNOs:

- FOV centers between *Aqua*-AIRS and *SNPP*-CrIS are within 8 km;
- Observations are made within 10 minutes;
- Both instruments observe within 3.3° of nadir, which corresponds with +/- 1 FOR of AMSU for AIRS or ATMS for CrIS.

2.3 Pixel-scale collocations of imagers and sounders:

Utilizing the multi-sensor capability at the pixel scale requires accurate and computationally efficient collocation of sounder and imager measurements. Various collocation methods exist (Schreier et al. 2010, Nagle and Holz 2009, Yue et al. 2013). In this study, the method developed by Wang et al. (2016) is applied by matching the instantaneous multi-sensor observations directly based on line-of-sight (LOS) pointing vectors, defined as the vector from the satellite position to the Earth surface pixel location. The details of this method and its accuracy are discussed at length in Wang et al. (2016).

In this study, the same collocation method is applied to both *Aqua* and *SNPP* to match the finer resolution imager pixels (MODIS and VIIRS) within a given sounder FOV (AIRS and CrIS). The LOS vectors are calculated using the geolocation datasets for different sensors, which contain latitude, longitude, satellite range, satellite azimuth and zenith angles. Collocation is performed using the criterion that the angular difference between the LOS vectors for sounder and imager should be less than half of the sounder FOV size angle. The CrIS FOV is treated as a 0.963° circle which corresponds to ~41% of the peak response and collects ~98% of total radiation falling on the detector (Wang et al. 2013). AIRS has a FOV half-power width of 1.1° (Fishbein et al. 2001). However, 0.963° is used for both AIRS and CrIS in the collocation. After obtaining collocation indices, the L2 cloud properties from both the imagers and sounders are populated accordingly. The high spatial resolution information from MODIS and VIIRS is retained using higher statistical moments and frequency distributions of cloud properties retrieved by imagers within collocated sounder FOV. These statistical metrics include the mean, standard deviation, skewness and kurtosis of MODIS and VIIRS cloud properties, the occurrence frequency of cloud types and cloud phase reported by the cloud mask and cloud thermodynamic phase variables, and joint histograms on the COD and CTP two-dimensional space following the convention of the International Satellite Cloud Climatology Project (ISCCP, Rossow and Schiffer 1999). In addition to summarizing fine imager spatial information over a coarser resolution sounder instrument, these statistical metrics physically describe a variety of cloud processes at both regional and global scales for a range of cloud types in different climate regimes, which are particularly relevant to sub-grid cloud parameterization in numerical models (e.g. Zhu and Zuidema 2009, Kawai and Teixeira 2010 and 2012, Kahn et al. 2017). The ISCCP-type of joint histograms have been widely used to dissect the uncertainty of the

cloud radiative forcing (e.g. Pincus et al. 2012) and climate feedback (e.g. Zelinka et al. 2012, Yue et al. 2016 and 2019) by cloud regimes (e.g. Oreopoulos et al. 2016).

By combining the SNOs and the sounder-imager collocated datasets, a multi-sensor multisatellite investigation is conducted to evaluate, at pixel scale, the self-consistency of cloud properties, to benchmark data continuity from the US polar-orbiting operational environmental satellites.

3. Results

Both *Aqua* and *SNPP* are in the 1:30 PM local equatorial crossing time sun-synchronous polar orbits, but at different altitudes. This altitude difference gives a ~2.667 day repeating pattern for AIRS and *SNPP*-CrIS observations at the same location. Accordingly, the number of SNOs between these two IR sensors varies with time and a large fraction are located at the high latitudes. In this study, seven focus days in January 2016 are selected for their large numbers of SNO pairs and the full operation for all four instruments. Table 2 lists the focus days and gives the number of observations obtained on each day. Figure 1 shows the latitudinal distribution of the focus day SNOs (black bars, y-axis on the left, Table 2). A significant number of observations (>2,500) are available at all latitudes, including the midlatitudes and tropics where SNOs are harder to obtain.

Fig. 2 shows the latitudinal variations of cloud frequency and zonal mean ECF and COD based on the data from the seven focus days. To determine the detection of clouds in the sounder FOV, two threshold values of ECF are used: 0.05 (solid lines) and 0.01 (dash lines). For MODIS and VIIRS, frequency of Cloudy, Uncertain cases as reported by the cloud mask variable is shown for MYD06 (black), MODIS continuity (red), and VIIRS continuity (blue) cloud products. Although it is difficult to directly compare the mean cloud properties retrieved by imagers and sounders,

AIRS V7 produces similar general patterns of latitudinal variation of cloud frequency with the imager products, which shows peaks of cloud occurrence in the tropics and midlatitude storm tracks, and troughs in the subtropics. However, CLIMCAPS V2 cloud retrievals do not show these variations, and its mean ECF values are much lower than AIRS V7 at all latitudes. A higher percentage of cloud frequency in the low latitude regions is reported by AIRS V7 than by imagers, consistent with previous findings showing higher sensitivity of hyperspectral IR sounders to optically thin clouds (Kahn et al. 2014, Yue et al. 2016). An increase of COD with latitude at mid to high latitude regions is detected by imagers, compared to a nearly flat or even decreasing mean ECF retrieved by the sounders. These differences will be further assessed in the following discussions.

3.1 Clouds retrieved by hyperspectral IR sounders

In Fig. 1, overlapped with the SNO count histograms are the occurrence frequency of sounder FOVs (colored lines, y-axis on the right) for four composites that satisfy the following four conditions, respectively: ECF $>$ 0.01(general cloudy condition), ECF $\leq$ 0.01 (clear or very thin clouds), ECF $>$ 0.8 (overcast or very thick clouds), and cases with successful CTP retrievals (QC for CTP is 0 or 1). These ECF values are selected based on the relationships between clouds and the IR sounder spectral information, as well as the retrieval uncertainty. The fraction of the highest quality atmospheric state retrievals below clouds, obtained from IR spectral information, decreases with higher ECF (Fetzer et al. 2006). The combination of IR and MW radiances can facilitate the retrieval of vertically resolved temperature and humidity profiles up to ECF of 0.7~0.8 (Yue et al. 2011, Yue and Lambrigtsen 2020, Yue et al. 2021). The ECF of 0.01 is often used as the threshold of cloud detection by IR sounders (e.g. Kahn et al. 2014). Moreover, it has been

356 shown that AIRS V7 cloud retrievals present higher uncertainty on thin, broken clouds and cloud
357 edges when ECF < 0.01 (Yue and Lambrigtsen 2020).

358 For each composite, the occurrence frequency is calculated as the percentage of AIRS or CrIS
359 FOVs with successful cloud retrievals that satisfy the composite condition relative to the total
360 number of FOVs in each latitudinal bin. The QC flags for each cloud parameter are reported in the
361 L2 products and used to determine whether the algorithm reports a successful cloud retrieval (when
362 QC = 0 or 1). Different colors are used to indicate retrieval algorithms for the two sounders. Since
363 AIRS V7 and CLIMCAPS retrieve cloud properties up to two cloud layers over each IR sounder
364 FOV, an effective CTP is calculated as the weighted mean CTP by the
365 ECF reported at each cloud layer.

366 These results show large differences between the AIRS V7 clouds with those from CLIMCAPS.
367 AIRS V7 produces a much larger number of cloudy observations (solid pink line in Fig. 1) and a
368 higher yield for CTP retrievals (dash dotted line, Fig. 1), except in the Antarctic region. The
369 magnitude of this difference reaches up to 30% over the Southern Hemisphere and the tropics.
370 Furthermore, AIRS V7 produces much more overcast or very thick clouds (dash lines, Fig. 1) but
371 fewer clear or very thin cloudy cases (dotted lines, Fig. 1) than CLIMCAPS, which is consistent
372 with smaller mean ECF and lower cloud frequency in the tropics and midlatitude storm track
373 regions by CLIMCAPS V2 in Fig. 2. As discussed previously, this is related to the differences
374 between the two algorithms for AIRS in cloud clearing and cloud retrieval QC, as well as the use
375 of different *a priori*. These differences are further evaluated in the following sections using the
376 imager observations.

377 Despite the differences of sensors, satellites, and spectral resolutions, the three CLIMCAPS

Version 2 retrievals evaluated in this study present similar latitudinal distributions of the cloud property distribution and cloud detection. As seen from Fig. 1, CLIMCAPS-*Aqua* (green dotted line) reports a higher percentage of clear or very thin cloudy cases than those for *SNPP* (yellow dotted line for CLIMCAPS-*SNPP* FSR and purple for CLIMCAPS-*SNPP* NSR), especially in the midlatitude region. Among the three CLIMCAPS products, CLIMCAPS-*Aqua* (green solid line) reports fewer cloudy cases than CLIMCAPS-*SNPP* (yellow and purple solid lines) in midlatitudes, but more cloudy cases in the tropics. The finer spectral resolution for CLIMCAPS-*SNPP* FSR retrievals produces a higher percentage of cloudy FOVs than the coarser spectral resolution radiances used by the NSR retrieval.

Figure 3 further characterizes the four IR sounder cloud retrievals using the joint distributions of observations among different algorithms. It is known that larger uncertainty of both sounder and imager retrievals exists over snow and ice covered surfaces (Chan and Comiso, 2013, Yue and Lambrigtsen 2020), so in this comparison the data points located in regions poleward of 60° are excluded. Cases are only included if both data products in the comparison (indicated by x- and yaxes of the plot) report valid retrievals. The three CLIMCAPS retrievals (x-axes) are compared with AIRS V7 (y-axes) for both ECF and CTP. The generally good agreement among the algorithms and sensors, especially for CTP, is encouraging, which shows the robustness of these products and consistency of information for clouds in hyperspectral IR sounders. However, CLIMCAPS reports a large number of cases with ECFs between 0 and 0.1, for which AIRS V7 reports ECFs ranging from 0 (clear sky) and 1 (completely cloudy). This issue is further illustrated in Fig. 4. For cases where CLIMCAPS-*Aqua* V2 retrieved ECF is less than 0.1, AIRS V7 (the magenta line) shows two peaks in the ECF occurrence frequency. The first peak is located at V7 ECF < 0.1, indicating the two algorithms agree with each other in cloud amount detection. The

larger second peak shows that more than 25% of cases with CLIMCAPS ECF < 0.1 have AIRS V7 ECF values of 0.8~0.9. As a result, the correlation coefficient (*r*) between ECF retrievals from AIRS V7 and CLIMCAPS V2 is only 0.27, which increases to 0.79 when neglecting ECF < 0.1 observations. Further separating the sounder FOVs into ice- and liquid-cloud-only categories shows that such inconsistency in cloud amount detection between the sounder algorithms exist in both categories as illustrated in Fig. S1 and S2. The sounder FOV is determined as ice/liquid-cloud-only when over 80% of collocated cloudy MODIS pixels are in ice/liquid thermodynamic phase in the MYD06 optical property cloud phase retrievals. Better agreements between sounder cloud products are found for ice-cloud-only FOVs.

A tighter agreement between CLIMCAPS V2 and AIRS V7 is seen for CTP retrievals as shown by points densely located along the identity line in Fig. 3. The correlation coefficients between CLIMCAPS-Aqua and AIRS V7 CTP are 0.69 for all cases and 0.92 for ECF > 0.1, respectively. High cloud cases (AIRS V7 CTP < 440hPa) show a much higher CTP correlation (r = 0.87) than for low clouds (AIRS V7 CTP > 600 hPa, r = 0.43). When both algorithms identify low clouds in the FOV, CLIMCAPS reports a slightly lower cloud top (larger CTP) than AIRS V7, with a median value difference of 12 hPa; whereas for high clouds, CLIMCAPS V2 reports a higher cloud top with its median CTP 13 hPa smaller than the one by AIRS V7.

In the next section, these differences among the various sounder cloud retrieval products are further evaluated using the cloud parameters determined by collocated MODIS and VIIRS data.

3.2 Comparison of sounder cloud properties and collocated imager measurements

Figures 5 and 6 compare the cloud properties retrieved from various sounder algorithms with the collocated imager cloud retrievals in the MYD06 and CLDPROP_MODIS products,

424 respectively. Comparisons with CLDPROP_VIIRS are similar to those using CLDPROP_MODIS
425 and hence are not shown in these figures. The cloud properties from MODIS pixels are averaged
426 within the collocated sounder FOV before this comparison.

427 The IR sounder retrieved ECF is positively correlated with the imager observed COD in the
428 top rows of Figs. 5 and 6, showing the consistency of cloud amount determined using different
429 sensors. However, two main differences are noticed. First, it is clear that the CLIMCAPS V2 (for
430 both *Aqua* and *SNPP*) misidentifies a significant number of cloudy cases as clear or thin clouds.
431 As shown in Fig. 4, more than 50% of these cases are optically thick clouds with large cloud
432 amount (ECF > 0.7) reported by AIRS V7 and COD values ranging from 2 to 10 by MODIS and
433 VIIRS. Secondly, the comparisons between CLIMCAPS and imager cloud products do not have
434 the cluster corresponding to cases with both high ECF and large COD values, as in the comparison
435 between AIRS V7 and imagers. As discussed previously, this is related to misidentification of
436 cloudy cases as clear or thin cloud conditions by CLIMCAPS. However, another main cause is that
437 CLIMCAPS cloud retrievals have the same QC flags as the physical atmospheric state retrievals;
438 as a result, cases with large cloud amount are filtered out. In general, AIRS V7 products exhibit
439 better agreement with MODIS and VIIRS in detecting cloud amount and occurrence. CLIMCAPS
440 V2 cloud retrievals could be further improved with better cloud clearing flow and more careful
441 treatment when retrieving clouds with unsuccessful atmosphere physical retrievals.

442 The sounder and imager CTP retrievals are also compared in the bottom rows of Fig. 5 and 6.
443 Despite instrument and algorithm differences, when both sounder and imager detect high clouds
444 (CTP < 440 hPa, including ECF < 0.1 cases), CTP retrievals agree with each other well. The
445 correlation coefficients with MYD06 CTP are 0.77, 0.52, and 0.62 for AIRS V7, CLIMCAPS*Aqua*,
446 and CLIMCAPS-*SNPP*-FSR, respectively. When imagers detect low clouds (CTP > 680 hPa), IR

447 sounders determine the majority of cases as low clouds but with a tail toward CTP values
448 corresponding to high and mid-level clouds (middle row). The disagreement mainly occurs when
449 sounder retrieved ECF is less than 0.1 as shown by the magenta contour lines. These are cases
450 when larger uncertainty in infrared cloud retrieval exists, as discussed previously. After removing
451 these cases, the sounder-imager discrepancy in the low cloud conditions is reduced greatly (bottom
452 row), especially for AIRS V7. These differences are consistent with the known limitation of
453 imagers such as MODIS, which tend to miss high and thin cloud layers (Holz et al. 2008) when
454 compared with AIRS (Kahn et al. 2014). However, the analysis presented here cannot completely
455 rule out the impact of uncertainty in the IR sounder cloud retrievals. When both hyperspectral
456 sounders and narrowband imagers detect low clouds, sounders tend to retrieve smaller CTP than
457 imager. For AIRS V7, the median difference in this condition is -65, -77, and -80 hPa with MYD06,
458 CLDPROP_MODIS, and CLDPROP_VIIRS products, respectively. The results are further
459 analyzed for ice- and liquid-cloud-only sounder FOVs (Fig. S3-S6), which are determined using
460 the same criteria as in the previous section. It is clear that the disagreements between the sounder
461 and imager CTP retrievals are mainly originated from the liquid-cloud-only sounder FOVs (Fig.
462 S5 and S6), while good agreements are found for ice-cloud-only conditions (Fig. S3 and S4).
463
464 3.3 Clouds retrieved by imagers
465 Figure 7 compares COD, CTP, and Re retrieved by different MODIS and VIIRS cloud
466 algorithms, with mean imager cloud properties over corresponding sounder FOVs are shown. Very
467 good agreement between MODIS and VIIRS, and between the MYD06 and continuity products is
468 seen. All correlation coefficients are greater than 0.8. For the three cloud parameters, correlation
469 is always the highest between products derived from the same instrument (MYD06 and

CLDPROP_MODIS), and the lowest between MYD06 and CLDPROP_VIIRS (but still reaching 0.81, 0.88, and 0.81 for COD, CTP, and Re, respectively) when both instrument and algorithm are different. From the same instrument MODIS but different algorithms, the correlation is lowest for CTP retrievals (r = 0.89) compared to COD (r = 0.97) and Re (r = 0.97). This is because MYD06 and the continuity cloud algorithm uses different methods and spectral channels to determine CTP, especially for cold clouds as shown in Fig. S7, where the correlation coefficients for CTPs from different imager cloud retrievals are less than 0.52 for ice-cloud-only conditions (Fig. S7) but larger than 0.79 for liquid-cloud-only cases (Fig. S8). However, a relationship near one-to-one is still seen clearly, indicating the consistency between the operational and continuity cloud products from MODIS, at least for the cloud properties averaged at the sounder resolution (~13.5km). Correlations between MODIS and VIIRS cloud products are lower than those from MODIS alone (with different algorithms), even when both products are derived from the same continuity algorithm. The degradation of agreement is larger for COD and Re than for CTP (Fig. 6). Separating results into ice- and liquid-cloud-only conditions, the COD (Re) correlation coefficients between the MODIS and VIIRS continuity cloud products are 0.84 (0.70) and 0.82 (0.75) for ice- and liquid-cloud-only conditions, respectively, as shown in Fig. S7 and S8. Although such good agreements between the two imagers are encouraging, the correlation for Re from the two CLDPROP products is lower than that for COD, with a much weaker correlation on the ice cloud Re retrievals. This reflects the effect of spectral channel and spatial resolution differences between MODIS and VIIRS, as well as the related adjustments made to the continuity algorithms, such as the liquid phase LUT for cloud microphysical retrievals, especially the impact of weaker ice crystal absorption at 2.25 μm (VIIRS) than at 2.13 μm (MODIS). Another possible factor is the collocation

492 error existing in the SNOs, but this is ruled out since results with more conservative collocation
493 criteria remain largely the same (not shown).

494 To further analyze the differences between the imager cloud products and the subpixel cloud
495 heterogeneity over the sounder FOVs, the standard deviation and skewness of the imager cloud
496 property distributions over the sounder FOVs are shown in Fig. 8 and 9, respectively. Correlations
497 are weaker in these higher statistical moments, yet for standard deviation they remain larger than
498 0.6. Similar to comparisons for mean values, tight one-to-one relationships are seen for standard
499 deviation at the sounder FOV scale between the two MODIS cloud products. Similar to mean value
500 comparisons, the CTP standard deviation has the lowest correlation coefficient ($r = 0.63$) compared
501 to the ones for COD ($r = 0.96$) and Re ($r = 0.87$), with a much lower correlation on CTP ($r = 0.44$)
502 for ice-cloud-only conditions (Fig. S9) but a high correlation ($r = 0.71$) for liquid-cloud-only FOVs
503 (Fig. S10). However, skewness only shows significant correlations for COD ($r = 0.78$) and Re (r
504 $= 0.70$) between the two MODIS datasets, but poor correlations ($r < 0.3$) for CTP. The impact from
505 the differences in CTP algorithms thus shows up more strongly on the higher statistical moments
506 and on cold cloud scenes. When evaluating data from different sensors, no correlation is seen for
507 skewness of any of the cloud parameters even with the same retrieval algorithms (Fig. 9, middle
508 and right columns), different from the comparisons using mean value and standard deviation (Figs.
509 7 and 8, middle and right columns).

510

511 3.4 Joint histograms, cloud types, and cloud thermodynamic phase

512 3.4.1 Cloud type by cloud property joint histograms

513 Figs. 10-13 show the two-dimensional cloud histograms calculated using SNOs from the focus
514 days over different surface types and regions, including the tropics (30°N~30°S), over ocean (land

fraction < 0.1, 60°N~60°S), over land (land fraction > 0.9, 60°N~60°S), and over ice and snow covered surfaces (frozen surfaces), respectively. The land fraction and surface classes are obtained from the AIRS V7 L2 product under variable names of landFrac and SurfClass, respectively. For MODIS and VIIRS, the ISCCP type of CTP-COD joint histograms are generated by summing the joint distributions over individual AIRS and CrIS FOV, with no averaging over sounder FOV. For AIRS and CrIS, joint distributions are calculated on the CTP and ECF space.

Consistent with results in previous sections, AIRS V7 shows peaks of both thin and thick clouds while CLIMCAPS V2 products show a single peak distribution of thin clouds. Better consistency of AIRS V7 with imager cloud products is also shown by the joint histograms. For example, in the tropics (Fig. 10) clusters corresponding to optically thick high clouds, thin cirrus, and broken or optically thin low clouds are seen in the AIRS V7 CTP-ECF histogram, consistent with the patterns in the MODIS and VIIRS CTP-COD histograms. Agreement between AIRS V7 and imager clouds is also found for mid-level and low cloud clusters over ocean (Fig. 11) and for high and mid-level clouds over land (Fig. 12). Over frozen surfaces (Fig. 13), the sounder clouds show optically thin and high clouds, especially in CLIMCAPS V2; a large percentage of mid-level clouds with medium to large ECF values are seen in AIRS V7, more consistent with the cloud histograms from imager observations. However, MODIS and VIIRS cloud detection and retrievals suffer a higher uncertainty over frozen surfaces (Chan and Comiso, 2013), and the small atmospheric thermal contrast with frozen surfaces presents additional challenges for hyperspectral IR sounder retrievals (Yue and Lambrigtsen 2020). Therefore, more accurate cloud measurements from in-situ or active space-borne instruments are needed to further quantify the quality of these imager and sounder cloud retrieval products in snow- and ice-covered regions.

Because of its long temporal coverage since 1999 when *Terra* MODIS began operating, high quality, and the distinct physical characteristics of different cloud types, the MODIS cloud data record, especially the CTP-COD joint histograms, have been widely used in different aspects of climate studies. These include detailed analyses on the radiative effect of different cloud types (Yue et al. 2016, Oreopoulos et al. 2016), evaluation of climate model simulations of clouds (Pincus et al. 2012), quantification of the cloud feedback by different cloud types (Zhou et al. 2014, Yue et al. 2019), and investigations of cloud impacts on hydrological cycle and the global circulation (Su et al. 2017), especially in the tropics. Therefore, the differences of the cloud frequency histograms from various imager retrieval products in the tropics are further analyzed here. In Fig. 14, the MODIS continuity product (depicted in Fig. 10) is used as the common base to evaluate the differences caused by algorithms and sensors: 1) between current NASA standard MODIS retrievals and the MODIS continuity algorithms, and 2) between the MODIS and VIIRS continuity cloud data records. The magnitude of joint frequency histogram differences is within ±5% using the focus day observations. MYD06 shows more clouds with CTP < 180 hPa but fewer low clouds with CTP > 800 hPa than the continuity product, consistent with findings in Platnick et al. (2021). VIIRS continuity cloud retrievals produce higher frequencies of clouds with COD between 9.4 and 60, but fewer high clouds with COD < 9.4. Whether and how these differences will impact the long-term trend and short-term variability of clouds as seen by the imagers warrants further study.

3.4.2 Cloud thermodynamic phase

Both MYD06 and continuity cloud products provide cloud thermodynamic phases (Table 1), given by the optical property retrieval (Cloud_Phase_Optical_Properties, in both MYD06 and continuity products) and the CLAVR-x processing system (Cloud_Phase_Cloud_Top_Properties,

560 continuity products only). The Cloud_Phase_Cloud_Top_Properties variable reports flags
561 determining pixels to be cloud free, water cloud, ice cloud, mixed phase cloud, or undetermined
562 phase. The Cloud_Phase_Optical_Properties flags indicate cloud mask not determined for pixel,
563 clear sky, liquid water cloud, ice cloud, or undetermined phase, the last of which includes mixed
564 phase clouds (Marchant et al. 2016). AIRS thermodynamic cloud phase, which is available in the
565 AIRS V6 and V7 Level 2 Support product, is based on a set of brightness temperature difference
566 and threshold tests using the channels in 960, 1231, 930, and 1227 cm^{-1} (Nasiri and Kahn 2008,
567 Kahn et al. 2014). These tests are applied to AIRS FOVs where ECF > 0.01, and classify the AIRS
568 FOV as containing liquid, ice, or unknown cloud phases. Detailed comparisons of AIRS cloud
569 phases with CALIPSO indicate good agreement with CALIPSO on ice phase detection, and
570 conservative liquid phase determination (Jin and Nasiri 2014, Peterson et al. 2020). These studies
571 also show that the unknown class of AIRS cloud phase corresponds to scenes containing both ice
572 and liquid particles, and low-level liquid clouds, especially in the trade-wind cumulus cloud regime.
573 Figs. 15-18 show the histograms of cloud thermodynamic phase (solid color bars for imagers
574 and magenta symbols for AIRS) for the same set of focus-day SNOs. Similar to joint histograms
575 in Fig. 10-13, each figure shows results over the four types of surfaces and regions: tropics, ocean,
576 land, and frozen surfaces. MODIS and VIIRS cloud mask histograms (hollow color bars) are also
577 shown in the figures, together with the frequency of clear sky detected by IR sounders (ECF < 0.01,
578 colored solid circles). Note that for MODIS and VIIRS, the mixed-phase or undetermined phase
579 category is shown with the y-axis on the right due to their much smaller frequency of occurrence.
580 For clear sky detection, the cloud-mask clear frequencies from all the imager products are similar
581 except over the frozen surfaces, where VIIRS cloud mask shows 10% higher frequency than
582 MODIS. For IR sounders, AIRS V7 produces significantly lower clear-sky frequency than

583 CLIMCAPS and imager cloud products over non-frozen surfaces. Over frozen surfaces, more
584 frequent clear conditions are reported by AIRS V7 than CLIMCAPS, although AIRS V7 is more
585 consistent with the clear frequency from MODIS and VIIRS data.

586 The frequencies of liquid or ice phase clouds are highly consistent between two cloud phase
587 variables in various imager cloud products, except for ice phase determination over frozen surfaces.
588 This is supported by the low uncertainty range of ice and liquid phase for these four conditions as
589 shown in Table 3. Here uncertainty is roughly characterized by the standard deviation of estimates
590 from different products and variables. The Cloud_Phase_Cloud_Top_Properties reports higher
591 percentage of liquid phase than Cloud_Phase_Optical_Properties. In particular, the VIIRS cloud
592 top cloud phase product always reports the highest frequency of liquid clouds. From both cloud
593 phase variables, MODIS reports more ice and fewer liquid clouds than VIIRS. When looking at
594 Cloud_Phase_Optical_Properties for MODIS, ice (liquid) cloud frequency is higher (lower) in
595 MYD06 than in the CLDPROP_MODIS products. The undetermined phase by the
596 Cloud_Phase_Optical_Properties includes both mixed and uncertain phases (Baum et al. 2012).
597 Except in tropics, MYD06 has the higher frequency of undetermined cases than the continuity
598 cloud products, and this is most prominent over the frozen surfaces with MYD06 reporting ~2.8%.

599 AIRS cloud phase retrievals report a higher frequency of ice clouds than imagers under all
600 conditions, especially in the tropics (Fig. 15) and over land (Fig. 17). However, a much lower
601 frequency of liquid clouds is retrieved by AIRS, which is consistent with a more conservative
602 liquid phase determination approach applied by AIRS cloud phase algorithm (Kahn et al. 2014).

603 The unknown phase of AIRS ranges from ~15% over the frozen surfaces to ~45% over ocean and
604 in the tropics, which corresponds with broken and thin low clouds and scenes with both ice and
605 liquid cloud particles (Jin and Nasiri 2014).
606
607 **4. Summary**
608 In this study, the pixel-scale collocation between the hyperspectral infrared (IR) sounders
609 (AIRS and CrIS) and high spatial resolution imagers (MODIS and VIIRS) is performed on the
610 pairs of Simultaneous Nadir Observations (SNOs) between *Aqua*-AIRS and *SNPP*-CrIS. Using
611 this approach, the cloud parameters retrieved by various algorithms for IR sounders and imagers
612 from different platforms are evaluated at the pixel level. Quantifying uncertainty in the cloud
613 observational data records is important for constraining the high uncertainty of clouds in weather
614 and climate research. This is also crucial in improving the retrieval of atmospheric, surface, and
615 radiation properties since satellite observations are highly subject to uncertainties and limitations
616 associated with cloud conditions in the instrument field of view (FOV) (e.g. Yue et al. 2013, Wong
617 et al. 2015, Tian et al, 2020). Moreover, narrowband imagers and hyperspectral sounders provide
618 important components of the long-term sustained observations of cloud properties in the Program
619 of Record (POR), as noted by the 2017 US National Academy Decadal Survey (ESAS 2017). The
620 analyses presented here will help to assess the capability of the POR, thus to identify potential gaps
621 existed in the POR for cloud properties.
622 Both the NASA standard and continuity retrieval algorithms for sounders and imagers are
623 investigated here in order to quantify the differences among the retrieval products, and to examine
624 the consistency and continuity of the data products from multiple sensors across different satellites.
625 This is essential to the goal of building a continuous record of satellite data using the *Terra*, *Aqua*,

626 *SNPP*, and *JPSS* series satellites, with sufficient quality to detect and quantify global
627 environmental change.

628 Multiple cloud parameters are analyzed (Table 1). Comparisons are made by investigating the
629 mean cloud parameters, and higher statistical moments of cloud property distributions measured
630 by MODIS and VIIRS over the corresponding AIRS and CrIS FOV. Cloud types indicated by the
631 joint histograms of cloud properties and cloud thermodynamic phases are included. Through these
632 comparisons, good agreement is found between the sounder and imager retrieved cloud products,
633 yet with distinct differences likely arising from algorithm and sensor differences. For IR sounders,
634 cloud top pressure (CTP) retrieved by AIRS Version 7 (V7) and CLIMCAPS (-*Aqua* and -*SNPP*)
635 Version 2 (V2) agree, as shown by correlation coefficients of 0.69 for all cases and 0.92 for cases
636 with effective cloud fraction (ECF) greater than 0.1, respectively. Compared to AIRS V7,
637 CLIMCAPS tends to produce a lower cloud top (CTP 12 hPa larger) for low clouds, but higher
638 cloud top (CTP 13 hPa smaller) for high clouds. However, CLIMCAPS V2 significantly
639 overestimates the frequency of clear and optically thin cloud (ECF < 0.1), relative to AIRS V7 and
640 imager products from both MODIS and VIIRS. This is due to the algorithmic differences between
641 CLIMCAPS V2 and AIRS V7 cloud retrieval algorithms. These differences include whether
642 iteration of cloud clearing is performed, the surface/atmospheric states used in the cloud retrieval,
643 the quality control procedures used, and different *a-priori* states used by AIRS V7 and CLIMCAPS.
644 How these differences affect the downstream atmospheric and surface retrievals in the two
645 algorithms, and the attribution of impacts from each factor, is beyond the scope of this study and
646 warrants further investigation.

647 High consistency is seen among different imager cloud products, especially in the mean and
648 standard deviation of cloud properties from the MODIS atmosphere cloud property retrieval

649 (MYD06) and the MODIS-VIIRS continuity cloud products (CLDPROP). The magnitude of the
650 correlation coefficients closely reflects the impact of algorithm differences and instrument spectral
651 and resolution differences, with highest correlations obtained between two MODIS products (same
652 sensor but different algorithms) and lowest between MYD06 and CLDPROP_VIIRS (different
653 sensors, different algorithms). The correlation coefficients are always higher for cloud optical
654 depth (COD) and particle effective radius (Re) than for CTP. For mean cloud properties, they are
655 as large as 0.97 between MYD06 and CLDPROP_MODIS, and 0.89 for CTP. For standard
656 deviations within the sounder FOV, the correlations are smaller than those for mean cloud
657 properties, ranging from 0.77 to 0.96 for COD, 0.66 to 0.97 for Re, but only 0.60 to 0.63 for CTP.
658 This is likely due to the fact that completely different CTP retrieval methods are used in the MODIS
659 operational and continuity cloud algorithms to accommodate the lack of near-IR and IR water
660 vapor and CO_2 absorption channels in VIIRS. Such algorithm and instrument impacts are more
661 apparent in the higher moment statistics of cloud properties such as skewness. The correlations of
662 COD and Re skewness between MYD06 and CLDPROP_MODIS drop to 0.78 and 0.70,
663 respectively. They are further reduced to below 0.4 when comparing MODIS and VIIRS cloud
664 products. For CTP skewness, the correlation coefficients are less than 0.3.

665 Two different cloud thermodynamic phase retrievals are available from imager observations,
666 which are obtained by the optical property retrieval (Cloud_Phase_Optical_Properties, in both
667 MYD06 and MODIS-VIIRS continuity products) and the CLAVR-x processing system
668 (Cloud_Phase_Cloud_Top_Properties, continuity products only). The frequencies of liquid or ice
669 phase clouds are very consistent between two cloud phase variables in different imager cloud
670 products, with uncertainty usually generally less than 4%. The largest uncertainty is reported for
671 ice phase determination over snow and ice covered surfaces. MODIS retrievals report more ice and

672 fewer liquid clouds than VIIRS, consistent with findings by Platnick et al. (2020). Comparing the
673 two different cloud phase retrievals, the Cloud_Phase_Cloud_Top_Properties reports higher
674 percentages of liquid phase than Cloud_Phase_Optical_Properties, and the
675 Cloud_Phase_Optical_Properties in MYD06 detects higher (lower) frequencies of ice (liquid)
676 clouds than that in the CLDPROP_MODIS products.

677 The general consistency of cloud observations among different sensors aboard *Aqua* and *SNPP*
678 from various algorithms is encouraging, especially for achieving a continuous multi-decadal
679 climate data record of clouds that can extend beyond the A-Train era and well into the 2030s with
680 the *JPSS* series. The quantification of algorithm differences has important implications for future
681 retrieval algorithm developments, and will further improve the capability and accuracy of such
682 climate data records.

683

684 **Data and Code Availability:**

685 MODIS (MYD06 10.5067/MODIS/MYD06_L2.061; MYD35
686 10.5067/MODIS/MYD35_L2.061; CLDPROP-MODIS
687 10.5067/VIIRS/CLDPROP_L2_MODIS_Aqua.011; CLDMSK-MODIS
688 10.5067/MODIS/CLDMSK_L2_MODIS_Aqua.001) and VIIRS data (CLDPROP-VIIRS
689 10.5067/VIIRS/CLDPROP_L2_VIIRS_SNPP.011; CLDMSK-VIIRS
690 10.5067/VIIRS/CLDMSK_L2_VIIRS_SNPP.001) were obtained through the Level-1
691 Atmosphere Archive and Distribution System (LAADS; http://ladsweb.nascom.nasa.gov/). AIRS
692 (AIRS V7 Level 2 Support Product 10.5067/APJ6EEN0PD0Z; CLIMCAPS-Aqua Version 2
693 Level 2 10.5067/JZMYK5SMYM86) and CrIS data (CLIMCAPS-SNPP Version 2 FSR

10.5067/62SPJFQW5Q9B; CLIMCAPS-SNPP Version 2 NSR 10.5067/8RUZI1F8U1UX) were obtained from the NASA Goddard Earth Sciences Data Information and Services Center (GESDISC) and could be accessed at https://earthdata.nasa.gov/. The collocation code is publicly available from https://github.com/wanglikun1973/CrIS_VIIRS_collocation. The data used to generate the figures and tables in this study can be obtained by contacting the corresponding author.

Author Contribution:

QY conceptualized the study, developed the methodology and datasets, carried out the formal analyses, and contributed to the writing of the manuscript. EF, BK, NS, JB, and BL contributed to the data curation, validation, investigation, and the writing of the manuscript. LW, IT, MM, and KM contributed to the data curation and software.

Competing Interests:

The authors declare that they have no conflict of interest

Acknowledgements:

The research was carried out at the Jet Propulsion Laboratory, California Institute of Technology, under a contract with the National Aeronautics and Space Administration (80NM0018D0004). QY, EJF, BHK, and BL were supported by NASA's Making Earth Science Data Records for Use in Research Environments (MEaSUREs) program. QY was supported by the NASA CloudSat and CALIPSO Science Team Recompete NNH15ZDA001N-CCST grant. QY, EJF, MS, and BHK acknowledge the support of the AIRS Project at JPL and the sounder SIPS at JPL.

References

Baum, B. A., Menzel, W. P., Frey, R. A., Tobin, D. C., Holz, R. E., Ackerman, S. A., Heidinger, A. K., and Yang, P.: MODIS Cloud-Top Property Refinements for Collection 6, *Journal of Applied Meteorology and Climatology*, *51*(6), 1145-1163, 2012.

Bony. S, and co-authors: *Clouds*, *circulation and climate sensitivity*. Nature Geoscience, 261-268, doi:10.1038/ngeo2398, 2015.

Borbas, E. E., G. Hulley, M. Feltz, R. Knuteson, and S. Hook: The Combined ASTER MODIS Emissivity over Land (CAMEL) Part 1: Methodology and High Spectral Resolution Application, *Remote Sensing*, 2018, 10, no. 4: 643, https://doi.org/10.3390/rs10040643.

Chahine, M. T.: Remote sounding of cloudy atmospheres. I. The single cloud layer*, J. Atmos. Sci., 31, 233–243, 1974.*

Chan, M. A., and Comiso, J. C.: Arctic Cloud Characteristics as Derived from MODIS, CALIPSO, and CloudSat, *Journal of Climate*, *26*(10), 3285-3306, 2013.

Eresmaa, R.: Imager-assisted cloud detection for assimilation of infrared atmospheric sounding interferometer radiances. *Q. J. R. Meteorol. Soc*. 140, 2342–2352, 2014.

ESAS 2017: National Academies of Sciences, Engineering, and Medicine (2018). Thriving on Our Changing Planet: A Decadal Strategy for Earth Observation from Space. Washington, DC: *The National Academies Press*. https://doi.org.10.17226/24938.

Feltz, M., Borbas, E., Knuteson, R., Hulley, G., Hook, S. The Combined ASTER MODIS Emissivity over Land (CAMEL) Part 2: Uncertainty and Validation. *Remote Sens.* **2018**, *10*, 664. https://doi.org/10.3390/rs10050664

Fetzer, E. J., Lambrigtsen, B. H., Eldering, A., Aumann, H. H., and Chahine, M. T.: Biases in total precipitable water vapor climatologies from Atmospheric Infrared Sounder and Advanced

741 Microwave Scanning Radiometer, J. Geophys. Res., 111, D09S16,
742 doi:10.1029/2005JD006598, 2006.
743 Fetzer, E. J., Yue, Q., Thrastarson, H. Th., and Ruzmaikin, A., ed., 2020: ALGORITHM
744 THEORETICAL BASIS DOCUMENT AIRS-Team Retrieval For Core Products and
745 Geophysical Parameters: Versions 6 and 7 Level2, available at:
746 https://docserver.gesdisc.eosdis.nasa.gov/public/project/AIRS/L2_ATBD.pdf
747 Fishbein, E., Lee, S-Y., and Fetzer, E. J., 2001: Atmospheric Infrared Sounder (AIRS) Level 2
748 Simulation System Description Document, available at:
749 http://asl.umbc.edu/pub/airs/jpldocs/sim/AIRS_L2_Simulation_Desc.pdf.
750 Frey, R. A., Ackerman, S. A., Holz, R. E., Steven, D., and Griffith, Z.: The Continuity
751 MODISVIIRS Cloud Mask, *Remote Sens.* 12, no. 20: 3334.
752 https://doi.org/10.3390/rs12203334, 2020.
753 Gelaro, R., McCarty, W., Suárez, M. J., Todling, R., Molod, A., Takacs, L., Randles, C. A.,
754 Darmenov, A., Bosilovich, M. G., Reichle, R., Wargan, K., Coy, L., Cullather, R., Draper,
755 C., Akella, S., Buchard, V., Conaty, A., da Silva, A. M., Gu, W., Kim, G.-K., Koster, R.,
756 Lucchesi, R., Merkova, D., Nielsen, J. E., Partyka, G., Pawson, S., Putman, W., Rienecker, M.,
757 Schubert, S. D., Sienkiewicz, M., and Zhao, B.: The modern-era retrospective analysis for
758 research and applications, Version 2 (MERRA-2), 30, 5419–5454,
759 https://doi.org/10.1175/JCLI-D-16-0758.1, 2017.
760 Gong, X., Li, Z., Li, J., Moeller, C. C., Cao, C., Wang, W., and Menzel, W. P.: Intercomparison
761 between VIIRS and CrIS by taking into account the CrIS subpixel cloudiness and viewing
762 geometry. *Journal of Geophysical Research: Atmospheres*, 123, 5335– 5345.
763 https://doi.org/10.1029/2017JD027849, 2018.

764 Heidinger, A. K., Evan, A. T., Foster, M. J., and Walther, A.: A naive Bayesian cloud detection
765 scheme derived from CALIPSO and applied with PATMOS-x, *J. Appl. Meteorol. Clim.*, 51,
766 1129–1144, 2012.
767 Heidinger, A. K., Foster, M. J., Walther, A., and Zhao,X.: The Pathfinder AtmospheresExtended
768 AVHRR climate dataset, B. Am. Meteorol. Soc., 95, 909-922, https://doi.org/10.1175/BAMS-
769 D-12-00246.1, 2014.
770 Holz, R. E., Ackerman, S. A., Nagle, F. W., Frey, R., Dutcher, S., Kuehn, R. E., Vaughan, M. A.
771 and Baum B.: Global Moderate Resolution Imaging Spectroradiometer (MODIS) cloud
772 detection and height evaluation using CALIOP, *J. Geophys. Res*., 113, D00A19,
773 doi:10.1029/2008JD009837, 2008.
774 Hook, S.: Combined ASTER and MODIS Emissivity database over Land (CAMEL) Emissivity
775 Monthly Global 0.05Deg V002,
776 https://doi.org/10.5067/MEASURES/LSTE/CAM5K30EM.002, 2019
777 IPCC (2013). Climate Change 2013: The Physical Science Basis. Contribution of Working
778 Group I to the Fifth Assessment Report of the Intergovernmental Panel on Climate Change
779 [Stocker, T.F., D. Qin, G.-K. Plattner, M. Tignor, S.K. Allen, J. Boschung, A. Nauels, Y.
780 Xia, V. Bex and P.M. Midgley (eds.)]. Cambridge University Press, Cambridge, United
781 Kingdom and New York, NY, USA, 1535 pp, doi:10.1017/CBO9781107415324, 2013.
782 Irion, F. W., Kahn, B. H., Schreier, M. M., Fetzer, E. J., Fishbein, E., Fu, D., Kalmus, P., Wilson,
783 R. C., Wong, S., and Yue, Q.: Single-footprint retrievals of temperature, water vapor and cloud
784 properties from AIRS, *Atmos. Meas. Tech*., 11, 971–995, https://doi.org/10.5194/amt11-971-
785 2018, 2018.

786 Jin, H. C., and Nasiri, S. L.: Evaluation of AIRS cloud-thermodynamic-phase determination with
787 *CALIPSO*. *J. Appl. Meteor. Climatol.*, 53, 1012–1027, https://doi.org/10.1175/JAMC-D-
788 130137.1, 2014.
789 Kahn, B. H., Irion, F. W., Dang, V. T., Manning, E. M., Nasiri, S. L., Naud, C. M., Blaisdell, J.
790 M., Schreier, M. M., Yue, Q., Bowman, K. W., Fetzer, E. J., Hulley, G. C., Liou, K. N.,
791 Lubin, D., Ou, S. C., Susskind, J., Takano, Y., Tian, B., and Worden, J. R.: The Atmospheric
792 Infrared Sounder version 6 cloud products, Atmos. Chem. Phys., 14, 399–426,
793 https://doi.org/10.5194/acp-14-399-2014, 2014.
794 Kahn, B. H., Schreier, M. M., Yue, Q., Fetzer, E. J., Irion, F. W., Platnick, S., Wang, C., Nasiri,
795 S. L., and L'Ecuyer, T. S.: Pixel-scale assessment and uncertainty analysis of AIRS and
796 MODIS ice cloud optical thickness and effective radius, *J. Geophys. Res. Atmos.*, 120,
797 11,669– 11,689, doi:10.1002/2015JD023950, 2015.
798 Kahn, B. H., Matheou, G., Yue, Q., Fauchez, T., Fetzer, E. J., Lebsock, M., Martins, J., Schreier,
799 M. M., Suzuki, K., and Teixeira, J.: An A-train and MERRA view of cloud, thermodynamic,
800 and dynamic variability within the subtropical marine boundary layer, Atmos. Chem. Phys., 17,
801 9451–9468, https://doi.org/10.5194/acp-17-9451-2017, 2017.
802 Kawai, H. and Teixeira, J.: Probability density functions of liquid water path and cloud amount of
803 marine boundary layer clouds: Geographical and seasonal variations and controlling
804 meteorological factors, J. Clim., 23, 2079–2092, 2010.
805 Kou, L., Labrie, D. and Chylek, P.: Refractive-indexes of water and ice in the 0.65- to 2.5-μm
806 spectral range. Appl. Opt. **1993**, 32, 3531–3540.
807 Li, J., Menzel, W. P., Sun, F., Schmit, T. J., and Gurka, J.: AIRS Subpixel Cloud

Characterization Using MODIS Cloud Products, *Journal of Applied Meteorology*, *43*(8), 1083-1094, 2004.

Manning, E. M., and Aumann H. H: Tropical simultaneous nadir observations for IR sounder evaluation and comparison, Proc. SPIE, Earth Observing Systems, 96070L (8 September 2015); https://doi.org/10.1117/12.2187151, 2015.

Marchant, B., Platnick, S., Meyer, K., Arnold, G. T., and Riedi, J: MODIS Collection 6 shortwave-derived cloud phase classification algorithm and comparisons with CALIOP. *Atmospheric Measurement Techniques*, *9*(4), 1587–1599. http://doi.org/10.5194/amt-9-1587-2016, 2016.

Masuda, K., Takashima, T. and Takayama, Y.: Emissivity of pure and sea waters for the model sea surface in the infrared window regions, Remote Sensing Environ. 24, 313–329. https://doi.org/10.1016/0034-4257(88)90032-6, 1988.

McCoy, D. T., Eastman, R., Hartmann, D. L., and Wood, R: The change in low cloud cover in a warmed climate inferred from AIRS, MODIS, and ERA-interim, Journal of Climate, 30(10), 3609-3620. https://dx.doi.org/10.1175/JCLI-D-15-0734.1, 2017.

Milstein, A.B., and Blackwell, W. J.: Neural network temperature and moisture retrieval algorithm validation for AIRS/AMSU and CrIS/ATMS, *J. Geophys. Res. Atmos.*, 121, 14141430, doi: 10.1002/2015JD024008, 2016.

Monarrez, R., ed., 2020: NASA-*SNPP* and NOAA-20 (JPSS-1) CLIMCAPS CrIS and ATMS Level-2 Products User Guide: File Format and Definition, available at: https://docserver.gesdisc.eosdis.nasa.gov/public/project/Sounder/CLIMCAPS.V2.README.pdf.

Nagle, F. W. and Holz, R. E.: Computationally Efficient Methods of Collocating Satellite, Aircraft, and Ground Observations, *J. Atmos. Oceanic Technol*. (2009) 26 (8):1585–1595, 2009.

Nasiri, S. L., and Kahn, B. H.: Limitations of bispectral infrared cloud phase determination and potential for improvement. *J. Appl. Meteor. Climatol.*, 47, 2895–2910, https://doi.org/10.1175/2008JAMC1879.1, 2008.

Nasiri, S. L., Dang, V. T., Kahn, B. H., Fetzer, E. J., Manning, E. M., Schreier, M. M., and Frey, R. A.: Comparing MODIS and AIRS Infrared-Based Cloud Retrievals, *Journal of Applied Meteorology and Climatology*, *50*(5), 1057-1072, 2011.

Oreopoulos, L., Cho, N., Lee, D., and Kato, S.: Radiative effects of global MODIS cloud regimes, *J. Geophys. Res. Atmos.*, 121, 2299– 2317, doi:10.1002/2015JD024502, 2016.

Oudrari, H., McIntire, J., Xiong, X., Butler, J., Lee, S., Lei, N., Schwarting, T., Sun, J.: Prelaunch radiometric characterization and calibration of the *SNPP* VIIRS sensor. *IEEE Trans. Geosci. Remote Sens*. **2015**, 53, 2195–2210, 2015.

Peterson, C. A., Yue, Q., Kahn, B. H., Fetzer, E., and Huang, X.: Evaluation of AIRS Cloud Phase Classification over the Arctic Ocean against Combined CloudSat–CALIPSO Observations, *Journal of Applied Meteorology and Climatology*, *59*(8), 1277-1294, 2020.

Pincus, R., Platnick, S., Ackerman, S. A., Hemler, R. S., and Patrick Hofmann, R. J.: Reconciling Simulated and Observed Views of Clouds: MODIS, ISCCP, and the Limits of Instrument Simulators, *Journal of Climate*, *25*(13), 4699-4720, 2012.

Platnick, S., Meyer, K. G., Yang, P., Ridgway, W. L., Riedi, J. C., King, M. D., Wind, G.,

Amarasinghe, N., Marchant, B., Arnold, G. T., et al.: The MODIS Cloud Optical and Microphysical Products: Collection 6 Updates and Examples from Terra and *Aqua*. *IEEE Trans. Geosci. Remote Sens*. **2017**, 55, 502–525, 2017.

Platnick, S., Meyer, K., Amarasinghe, N., Wind, G., Hubanks, P. A. and Holz, R. E.: Sensitivity of Multispectral Imager Liquid Water Cloud Microphysical Retrievals to the Index of Refraction, *Remote Sensing* 12, no. 24: 4165. https://doi.org/10.3390/rs12244165, 2020.

Platnick, S., Meyer, K., Wind, G., Holz, R. E., Amarasinghe, N., Hubanks, P. A., Marchant, B., Dutcher, S., and Veglio, P.: The NASA MODIS-VIIRS Continuity Cloud Optical Properties Products. *Remote Sens.* 13, no. 1: 2. https://doi.org/10.3390/rs13010002, 2021.

Rossow, W. B., and Schiffer, R. A.: Advances in understanding clouds from ISCCP. *Bull. Amer. Meteor. Soc*., 80, 2261–2287, https://doi.org/10.1175/15200477(1999)080,2261:AIUCFI.2.0.CO;2, 1999.

Schreier, M. M.; Kahn, B. H.; Eldering, A.; Elliott, D. A.; Fishbein, E.; Irion, F. W.; Pagano, T. S.: Radiance comparisons of MODIS and AIRS using spatial response information. *J. Atmos. Oceanic Technol.* 2010, 27, 1331–1342, 2010.

Seemann, S. W., Borbas, E. E., Knuteson, R. O., Stephenson, G. R., and Huang, H.-L.: Development of a Global Infrared Land Surface Emissivity Database for Application to Clear Sky Sounding Retrievals from Multi-spectral Satellite Radiance Measurements. *J. Appl. Meteor. Climatol.*, Vol. 47, 108-123, 2008.

Smith, N. and Barnet, C.D.: Uncertainty Characterization and Propagation in the Community Long-Term Infrared Microwave Combined Atmospheric Product System (CLIMCAPS). *Remote Sens.* **2019**, *11*, 1227, 2019.

873 Smith, N. and Barnet, C. D.: CLIMCAPS observing capability for temperature, moisture, and trace
874 gases from AIRS/AMSU and CrIS/ATMS, 13, 4437–4459, https://doi.org/10.5194/amt-
875 13-4437-2020, 2020.
876 Smith, N., Esmaili, R., and Barnet, C. D. 2021: Community Long-Term Infrared Microwave
877 Combined Atmospheric Product System (CLIMCAPS) Science Application Guides,
878 available at:
879 https://docserver.gesdisc.eosdis.nasa.gov/public/project/Sounder/CLIMCAPS_V2_L2_scienc
880 e_guides.pdf.
881 Su, H., and Coauthors: Tightening of Hadley ascent and tropical high cloud region key to
882 precipitation change in a warmer climate. *Nat. Commun*., 8, 15771,
883 https://doi.org/10.1038/ncomms15771, 2017.
884 Susskind, J., Barnet, C. D., and Blaisdell, J. M.: Retrieval of atmospheric and surface parameters
885 from AIRS/AMSU/HSB data in the presence of clouds, *IEEE Trans. Geosci. Remote Sens.,* 41,
886 390–409, 2003.
887 Susskind, J., Barnet, C., Blaisdell, J., Iredell, L, Keita, F., Kouvaris, L. Molnar, G., and Chahine,
888 M.: Accuracy of geophysical parameters derived from Atmospheric Infrared
889 Sounder/Advanced Microwave Sounding Unit as a function of fractional cloud cover, *J.*
890 *Geophys. Res.*, 111, *D09S17, doi:*10.1029/2005JD006272, 2006.
891 Susskind, J., Blaisdell, J. M., and Iredell, L: Improved methodology for surface and atmospheric
892 soundings, error estimates, and quality control procedures: the atmospheric infrared sounder
893 science team version-6 retrieval algorithm, *Journal of Applied Remote Sensing* 8(1), 084994
894 (31 March 2014). https://doi.org/10.1117/1.JRS.8.084994, 2014.
895 Tian, B., and Hearty, T.: Estimating and removing the sampling biases of the AIRS Obs4MIPs

V2 data. *Earth and Space Science*, 7, e2020EA001438. https://doi.org/10.1029/2020EA001438, 2020.

Thrastarson, H. Th., Fetzer, E. F., Ray, S., Hearty, T., and Smith, N., 2021: Overview of the AIRS Mission: Instruments, Processing Algorithms, Products, and Documentation, 2nd Edition. Available from: https://docserver.gesdisc.eosdis.nasa.gov/public/project/AIRS/Overview_of_the_AIRS_Mission.pdf

Thrastarson, H. Th., ed., 2021: AIRS/AMSU/HSB Version 7 Level 2 Product User Guide. Available at: https://docserver.gesdisc.eosdis.nasa.gov/public/project/AIRS/V7_L2_Product_User_Guide.pdf.

Tobin, D. C., Revercomb, H. E., Moeller, C. C., Pagano, T. S: Use of atmospheric infrared sounder high–spectral resolution spectra to assess the calibration of moderate resolution imaging spectroradiometer on EOS *Aqua*. *J. Geophys. Res. Atmos*. 2006, 111, 2006.

Wagner, R.; Benz, S.; Möhler, O.; Saathoff, H.; Schnaiter, M.; Schurath, U.: Mid-infrared Extinction Spectra and Optical Constants of Supercooled Water Droplets. J. Phys. Chem. A **2005**, 109, 7099–7112.

Wang, L., Tremblay, D. A., Han, Y., Esplin, M., Hagan, D. E., Predina, J., Suwinski, L., Jin, X., Chen, Y.: Geolocation assessment for CrIS sensor data records. *J. Geophys. Res. Atmos.* 2013,118, 690–704, 2013.

Wang, L., Tremblay, D., Zhang, B., Han, Y.: Fast and Accurate Collocation of the Visible Infrared Imaging Radiometer Suite Measurements with Cross-Track Infrared Sounder, *Remote Sens.* 8, no. 1: 76. https://doi.org/10.3390/rs8010076, 2016.

Wang et al., ed., 2021: Test Report of Performance of CLIMCAPS-*SNPP* and CLIMCAPS-JPSS1 Retrievals, available at: https://docserver.gesdisc.eosdis.nasa.gov/public/project/Sounder/CLIMCAPS.V2.Test.Report.pdf.

Wong, S., Fetzer, E. J., Schreier, M., Manipon, G., Fishbein, E. F., Kahn, B. H., Yue, Q., and Irion, F. W.: Cloud-induced uncertainties in AIRS and ECMWF temperature and specific humidity, *J. Geophys. Res.*, 120, doi:10.1002/2014JD022440, 2015.

Wu, X. and Smith, W. L.: Emissivity of rough sea surface for 8–13 μm: modeling and verification, Appl. Opt. **36**, 2609-2619. https://doi.org/10.1364/AO.36.002609, 1997.

Yao, Z., Li, J. and Zhao, Z.: Synergistic use of AIRS and MODIS for dust top height retrieval over land. *Adv. Atmos. Sci.* **32,** 470–476, 2015. https://doi.org/10.1007/s00376-014-4046-y.

Yue, Q., Kahn, B. H., Xiao, H., Schreier, M. M., Fetzer, E. J., Teixeira, J., and Suselj, K.: Transitions of cloud-topped marine boundary layers characterized by AIRS, MODIS, and a large eddy simulation model. Journal of Geophysical Research-Atmospheres, 118(15), 8598-8611, 2013.

Yue, Q., Kahn, B. H., Fetzer, E. J., and Teixeira, J.: Relationship between marine boundary layer clouds and lower tropospheric stability observed by AIRS, CloudSat, and CALIOP. *Journal of Geophysical Research-Atmospheres*, 116, 2011.

Yue, Q., Fetzer, E. J., Kahn, B. H., Schreier, M., Wong, S., Chen, X., and Huang, X.: Observation-based Longwave Cloud Radiative Kernels Derived from the A-Train, *J. Climate*, 29(6), 2023–2040, doi: http://dx.doi.org/10.1175/JCLI-D-15-0257.1, 2016.

Yue, Q., Kahn, B. H., Fetzer, E. J., Wong, S., Frey, R., and Meyer, K. G.: On the response of MODIS cloud coverage to global mean surface air temperature. Journal of Geophysical

942 Research-Atmospheres, 122(2), 966-979, 2017.
943 Yue, Q., Fetzer, E. J., Kahn, B. H., Wong, S., Huang, X., and Schreier, M.: Temporal and Spatial
944 Characteristics of Short-term Cloud Feedback on Global and Local Interannual Climate
945 Fluctuations from A-Train Observations, *J. Climate*, DOI: https://doi.org/10.1175/JCLI-D18-
946 0335.1, 2019.
947 Yue, Q., and Lambrigtsen, B. ed., 2017: AIRS V6 Test Report Supplement: Performance of
948 AIRS+AMSU vs. AIRS-only Retrievals, available at:
949 https://docserver.gesdisc.eosdis.nasa.gov/repository/Mission/AIRS/3.3_ScienceDataProduct
950 Documentation/3.3.5_ProductQuality/V6_Test_Report_Supplement_Performance_of_AIRS
951 +AMSU_vs_AIRS-Only_Retrievals.pdf.
952 Yue, Q., and Lambrigtsen, B. ed., 2020: AIRS V7 L2 Performance Test and Validation Report,
953 available at:
954 https://docserver.gesdisc.eosdis.nasa.gov/public/project/AIRS/V7_L2_Performance_Test_an
955 d_Validation_report.pdf.
956 Yue, Q. et al., ed., 2021: Version 2 CLIMCAPS-*Aqua* Retrieval Product Performance Test
957 Report, available at:
958 https://docserver.gesdisc.eosdis.nasa.gov/public/project/Sounder/CLIMCAPS.V2.Test.Repor
959 t.*Aqua*.pdf.
960 Zelinka, M. D., Klein, S. A., and Hartmann D. L.: Computing and Partitioning Cloud Feedbacks
961 Using Cloud Property Histograms. Part I: Cloud Radiative Kernels. *J. Climate*, 25, 3715–3735,
962 2012.
963 Zhu, P., and Zuidema, P.: On the use of PDF schemes to parameterize sub-grid clouds, *Geophys.*
964 *Res. Lett.*, 36, L05807, doi:10.1029/2008GL036817, 2009.

916 Table 1: The satellite cloud parameters examined in this study, and the retrieval algorithms 917 and products from which these parameters are obtained.

Satellite	Sensor	Retrieval Algorithm / Product (Nadir Spatial Resolution in km)	Cloud Parameters
Aqua	AIRS	AIRS Version 7 Level 2 Standard and Support Product (13 km)	• Effective Cloud Fraction (ECF) • Cloud Top Pressure (CTP) • Cloud Thermodynamic Phase
		Version 2 CLIMCAPS-*Aqua* Level 2 Infrared and Microwave Combined Retrieval (13 km)	• Effective Cloud Fraction (ECF) • Cloud Top Pressure (CTP)
	MODIS	Collection 6.1 *Aqua* MODIS Atmosphere Level 2 Cloud Product (MYD35, MYD06) (1 km)	• Cloud Mask • Cloud Top Pressure (CTP) • Cloud Optical Depth (COD) • Cloud Effective Radius (Re) • Cloud Phase Optical Properties
		Version 1.1 NASA MODIS Continuity Cloud Mask and Cloud Property Products (CLDMSK/CLDPROP_MODIS) (1 km)	• Cloud Mask • Cloud Top Pressure (CTP) • Cloud Optical Depth (COD) • Cloud Effective Radius (Re) • Cloud Phase Optical Properties • Cloud Phase Cloud Top Properties
SNPP	CrIS	Version 2 CLIMCAPS-*SNPP* Full Spectral Resolution (FSR) Level 2 Retrieval (13 km)	• Effective Cloud Fraction (ECF) • Cloud Top Pressure (CTP)
		Version 2 CLIMCAPS-*SNPP* Nominal Spectral Resolution (NSR) Level 2 Retrieval (13 km)	• Effective Cloud Fraction (ECF) • Cloud Top Pressure (CTP)
	VIIRS	Version 1.1 NASA VIIRS Continuity Cloud Mask and Cloud Property Products (CLDMSK/CLDPROP_VIIRS) (0.75 km)	• Cloud Mask • Cloud Top Pressure (CTP) • Cloud Optical Depth (COD) • Cloud Effective Radius (Re) • Cloud Phase Optical Properties • Cloud Phase Cloud Top Properties

921

922 Table 2 Number of SNOs between *Aqua*-AIRS and *SNPP*-CrIS on the seven focus days used
923 in this study.
924

Focus Day	Jan. 01, 2016	Jan. 03, 2016	Jan 04, 2016	Jan 09, 2016	Jan 11, 2016	Jan 14, 2016	Jan 17, 2016
# of SNOs	10,000	10,000	1372	10,000	10,000	10,000	8,903

925

926

927 Table 3. The mean value and uncertainty range of the occurrence frequencies of ice and liquid
928 phase clouds based on the cloud thermodynamic phase variables from the three imager cloud
929 retrievals: MYD06, CLDRPOP_MODIS, and CLDPROP_VIIRS. Results over the five types of
930 surfaces and regions are shown respectively for tropics, ocean, land, frozen surfaces, and global.
931 For each condition, five estimates of cloud phase frequencies are available based on two types of
932 imager-derived cloud thermodynamic phase: Cloud_Phase_Optical_Properties determined by the
933 optical property retrieval (provided in both MYD06 and the two continuity products), and
934 Cloud_Phase_Cloud_Top_Properties obtained through the CLAVR-x processing system applied
935 in the continuity cloud algorithm (provided in the CLDPROP-MODIS and -VIIRS cloud products).
936 The uncertainty range is characterized by the standard deviation of the five estimates obtained in
937 each region.
938

Frequency (%)	Tropics (30°N~30°S)	60°N~60°S Ocean	60°N~60°S Land	Frozen Surfaces	Global, All Cases
Liquid Phase	37.64±3.21	53.94±3.50	35.16±2.81	14.03±1.10	44.27±2.79
Ice Phase	26.36±1.96	21.32±2.59	23.37±1.03	14.28±4.38	20.43±3.02

939

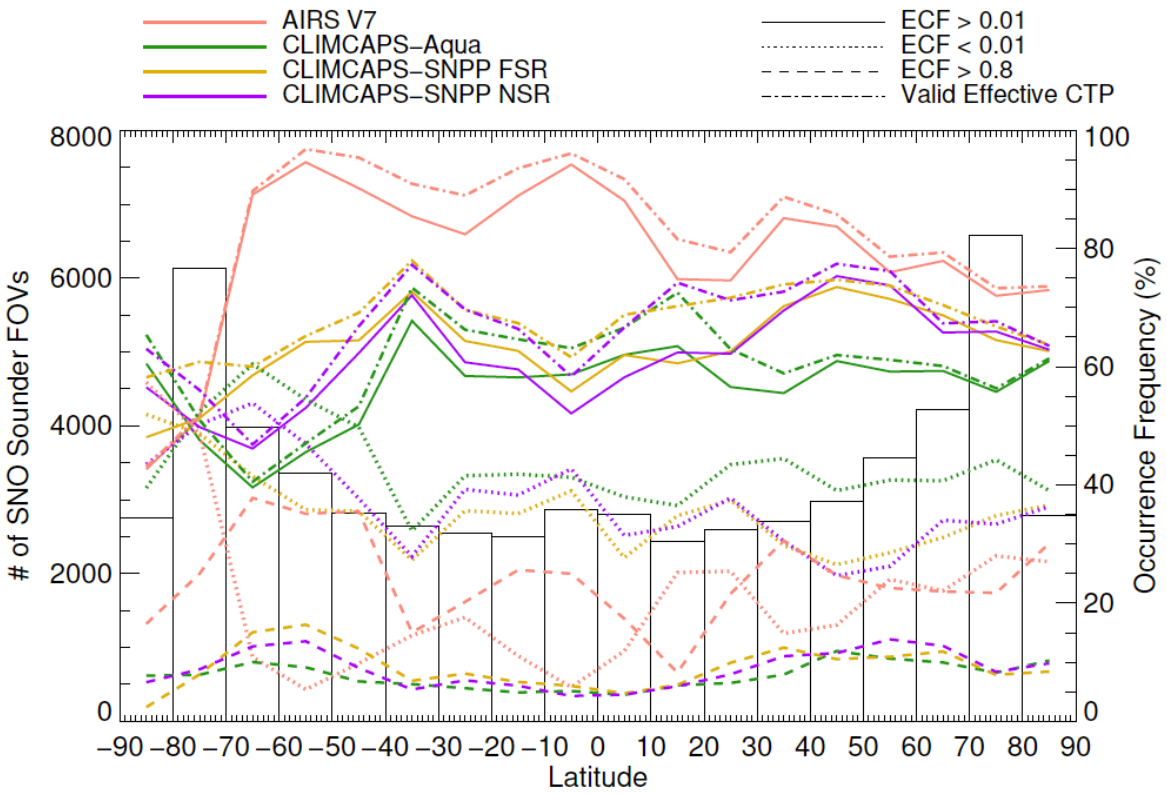

Figure 1. The latitudinal distribution of the SNO pairs for *Aqua*-AIRS and *SNPP*-CrIS (black bars) and the occurrence frequencies of various sounder retrieved cloud parameters (right yaxis, %) for four composites that satisfy the following four conditions, respectively: ECF > 0.01(solid lines, general cloudy condition), ECF ≤ 0.01 (dotted lines, clear or very thin clouds), ECF > 0.8 (dash lines, overcast or very thick clouds), and cases with successful CTP retrievals (dash dotted lines, QC for CTP is 0 or 1). Data from the seven focus days are used (see Table 2) and binned by latitude of the sounder FOVs in 10° latitude bins. Four different sounder retrieval products are shown by colored lines: AIRS Version 7 (AIRS V7, pink), CLIMCAPS-*Aqua* (green), CLIMCAPS-*SNPP* FSR (yellow), and CLIMCAPS-*SNPP* NSR (purple). Occurrence frequency is calculated as the percentage of AIRS or CrIS FOVs with successful cloud retrievals (quality control indicator = 0 or 1) satisfying the aforementioned four conditions to the total number of FOVs in each latitudinal bin.

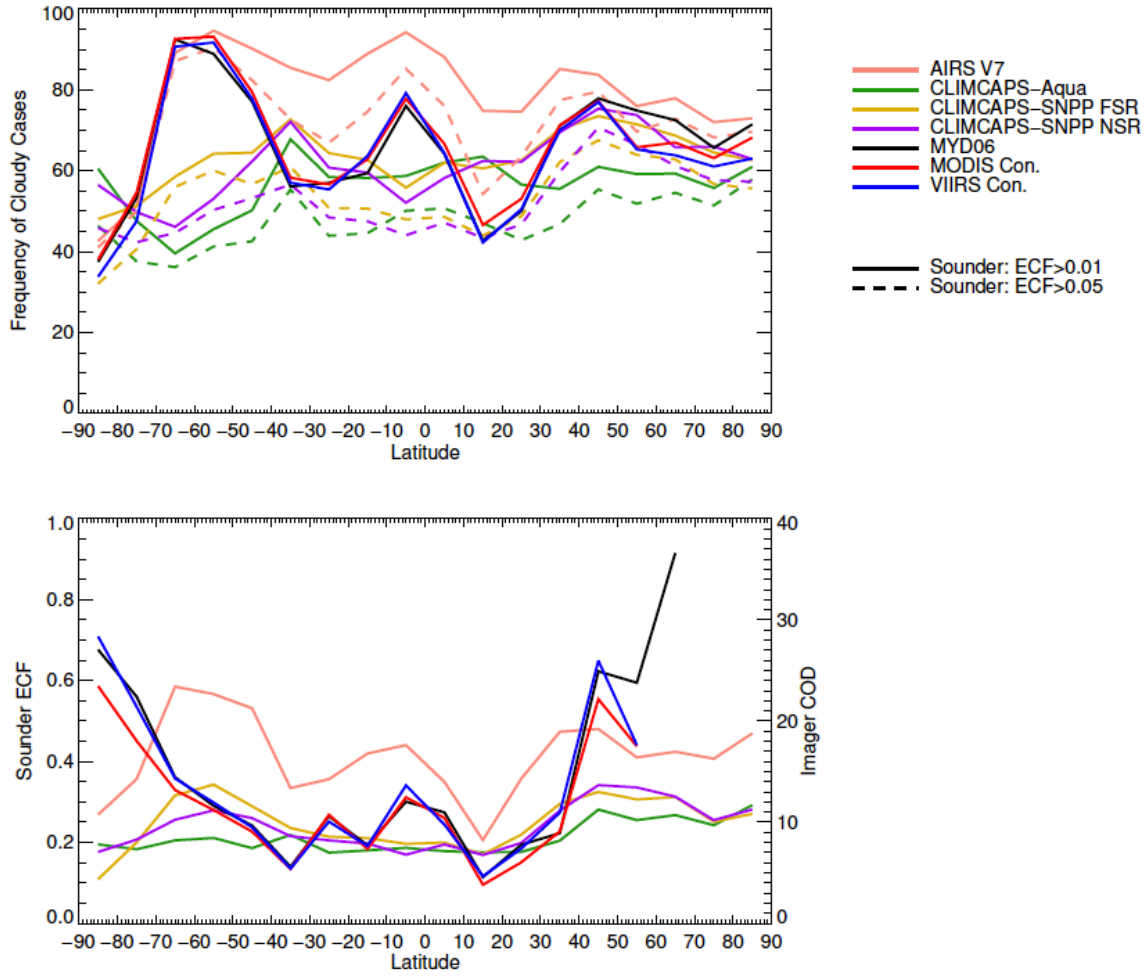

Figure 2. a) Zonal mean frequency of cloudy cases as observed by hyperspectral sounders and imagers. For MODIS and VIIRS, frequency of Cloudy, Uncertain cases as reported by cloud mask is shown for MYD06 (black), MODIS continuity (red), and VIIRS continuity (blue) cloud products. For AIRS and CrIS, solid and dash lines show frequencies of sounder FOVs with ECF > 0.01 and ECF > 0.05, respectively. Results for AIRS Version 7 (AIRS V7, pink), CLIMCAPS-*Aqua* (green), CLIMCAPS-*SNPP* FSR (yellow), and CLIMCAPS-*SNPP* NSR (purple) are shown for sounder cloud products. b) Zonal mean values of sounder ECFs (left y axis) and imager COD (right y axis) from these retrieval algorithms.

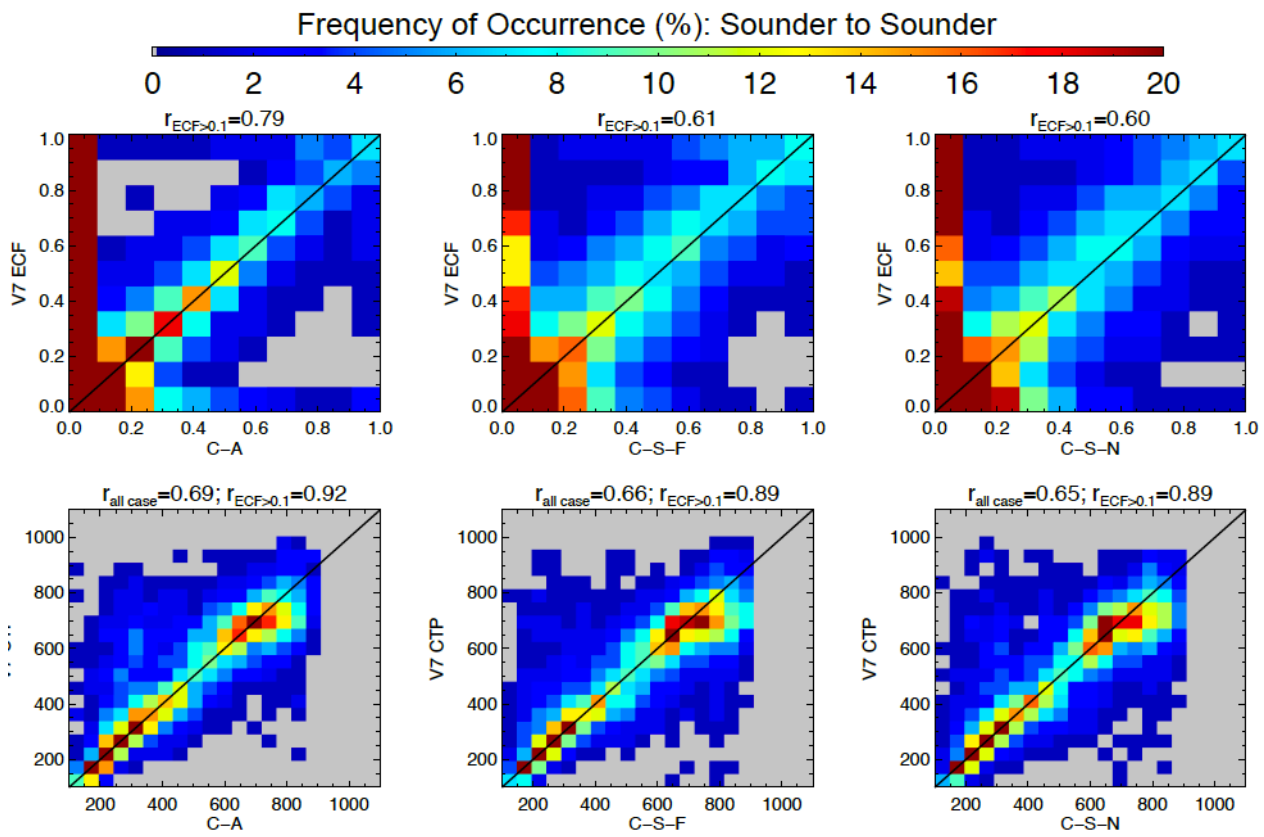

Figure 3. Comparisons of ECF (top row) and effective CTP (bottom row) derived from different sounder retrieval algorithms. Linear correlation coefficients are calculated for cloud properties obtained from retrieval products indicated on the axes and are given on top of the each plot. From left to right, results comparing AIRS Version 7 with CLIMCAPS-*Aqua* (C-A), CLIMCAPS-*SNPP* FSR (C-S-F), and CLIMCAPS-*SNPP* NSR (C-S-N) are shown using joint distributions of frequency of occurrence (%). The data points located in regions poleward of 60° are excluded. Cases are included only when both retrievals in comparison (x- and y-axes of the plot) report valid retrievals.

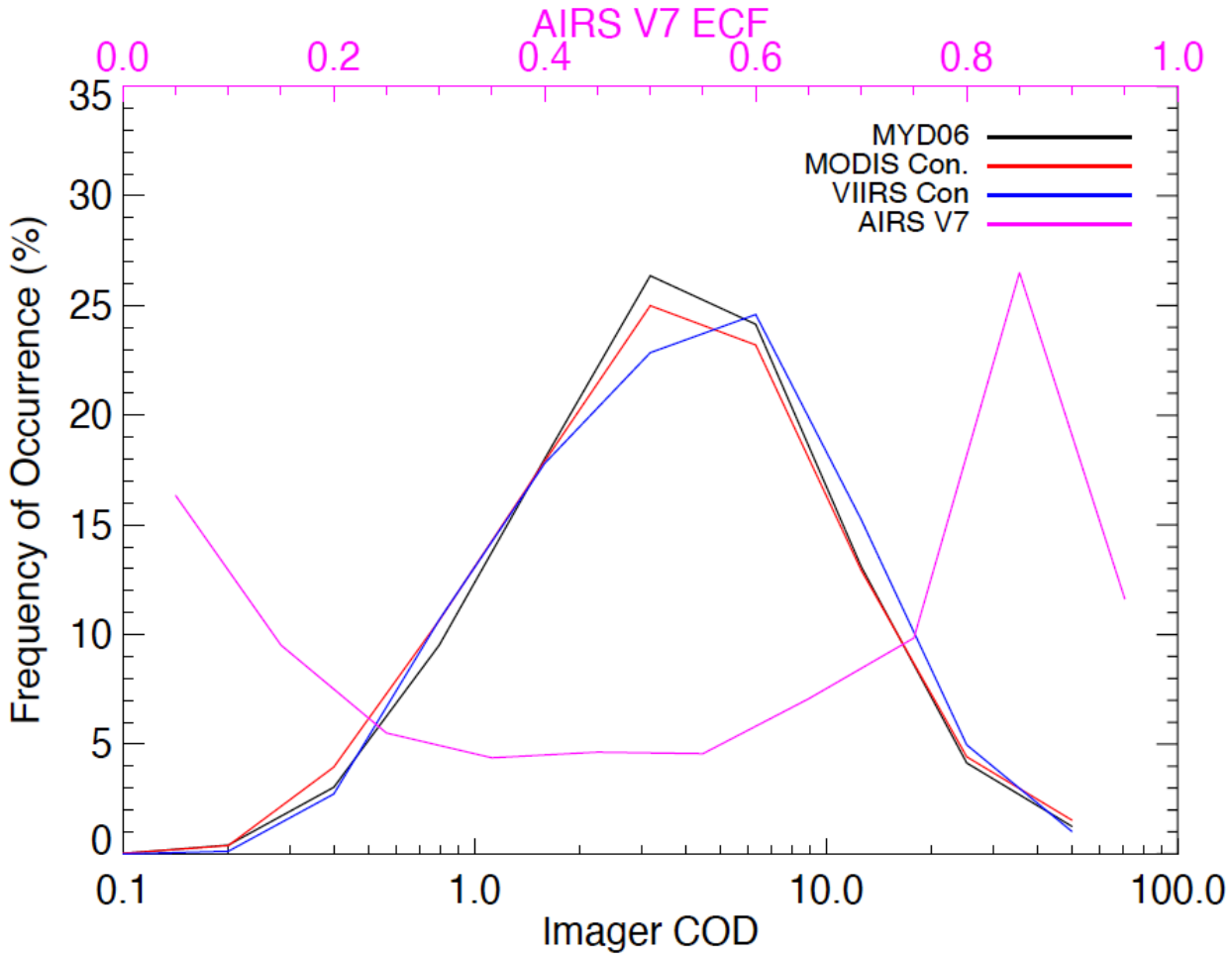

Figure 4. Frequency histograms showing the density distributions of imager cloud optical depth (COD, bottom x-axis) and AIRS V7 ECF (magenta, upper x-axis) for cases where V2 CLIMCAPS-*Aqua* retrieves an ECF value less than 0.1. Different imager cloud products are included: MYD06 (black), *Aqua*-MODIS continuity cloud products (MODIS Con., red), and *SNPP*-VIIRS continuity cloud products (VIIRS Con., blue).

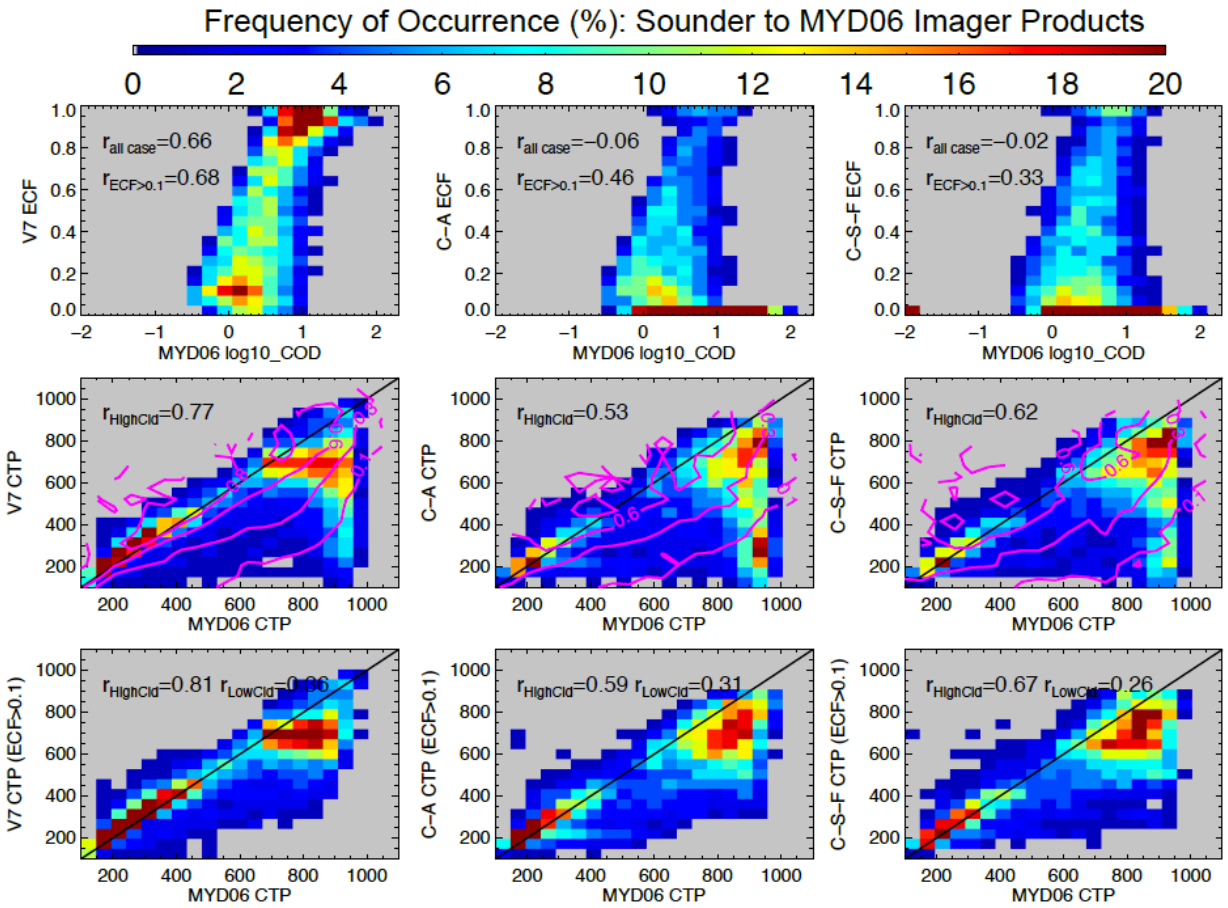

Figure 5. Comparisons of sounder and imager derived cloud properties shown by joint distribution of case frequency of occurrence. Top row shows evaluation of sounder-derived ECF by cloud optical depth (COD, in log10 scale) from the MYD06 products. The middle row compares the sounder effective CTP with CTP from MYD06 overlaid by the magenta contours showing the mean ECF from the corresponding sounder retrievals. The bottom row is similar to the middle row except that the cases with sounder ECF < 0.1 are removed from the comparison. Different sounder retrieval algorithms are included. From left to right, data from AIRS Version 7, CLIMCAPS-*Aqua* (C-A), and CLIMCAPS-*SNPP* FSR (C-S-F) are used. The data points located in regions poleward of 60° are excluded. Cases are included only when both retrievals in comparison (x- and y-axes of the plot) report valid retrievals. The cloud properties from MODIS pixels collocated within the

same sounder FOV are averaged before comparing with the IR sounder data. Linear correlation coefficients between the variables on x- and y-axes for different conditions are given in each plot.

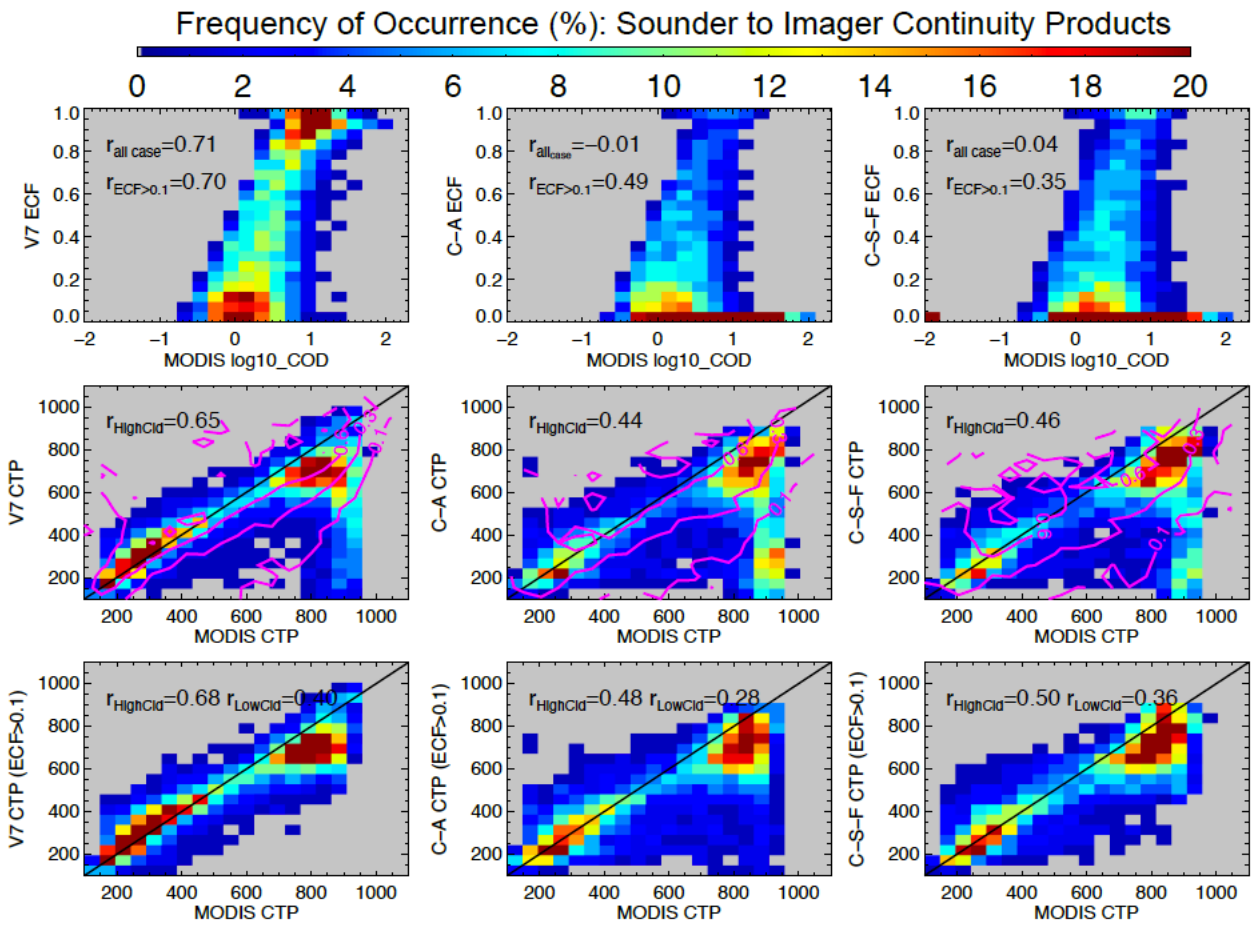

Figure 6. Similar to Fig. 5, except using the MODIS continuity cloud product (CLDPROP_MODIS).

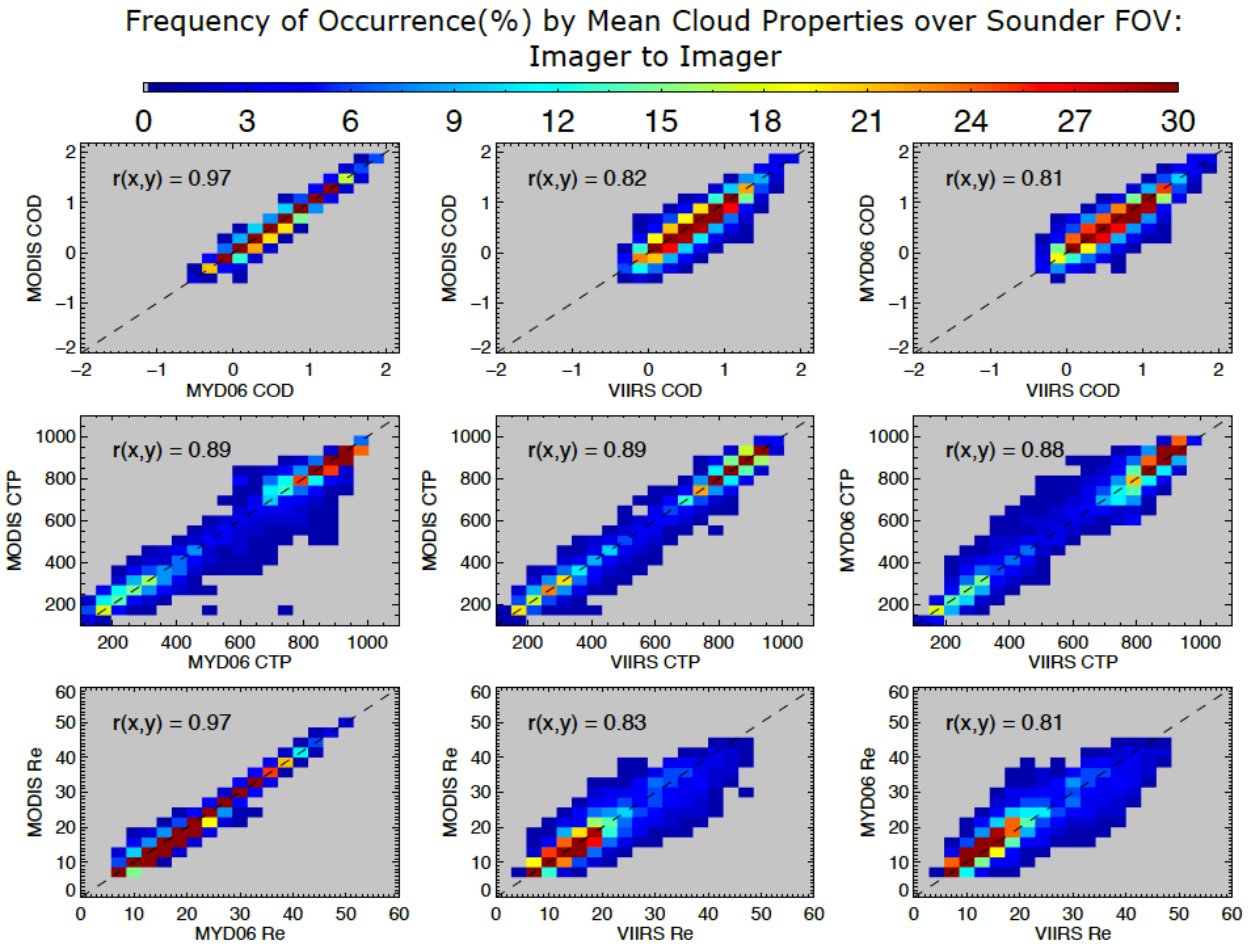

Figure 7. Comparison of cloud optical depth (COD, in log10 scale), cloud top pressure (CTP, hPa), and effective particle size (Re, μm) retrieved by MODIS and VIIRS cloud algorithms. The mean imager cloud properties over corresponding sounder FOVs are compared over the SNOs. From left to right show the results of following comparisons: *Aqua* MODIS continuity cloud products

(CLDPROP_MODIS) with MYD06, CLDPROP_MODIS with *SNPP*-VIIRS continuity cloud products (CLDPROP_VIIRS), and MYD06 with CLDPROP_VIIRS, respectively. Linear correlation coefficients between the variables on x- and y-axes are given in each plot.

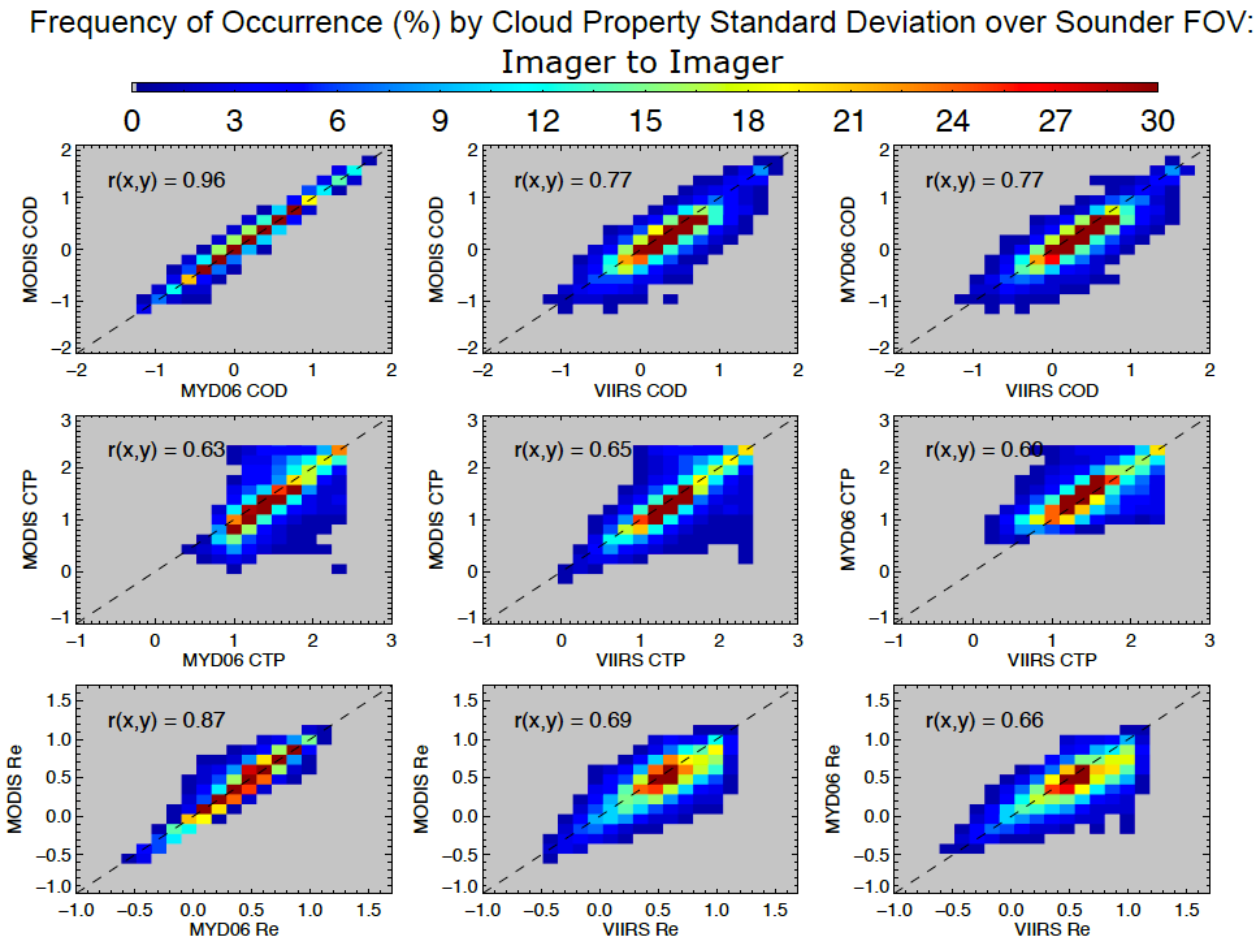

Figure 8. Similar to Fig. 7, except showing comparisons of standard deviation of cloud properties over the sounder FOV, which are calculated using the finer resolution imager observations collocated with the same sounder FOV. All the results are presented on log10 scale. Linear correlation coefficients between the variables on x- and y- axes are given in each plot.

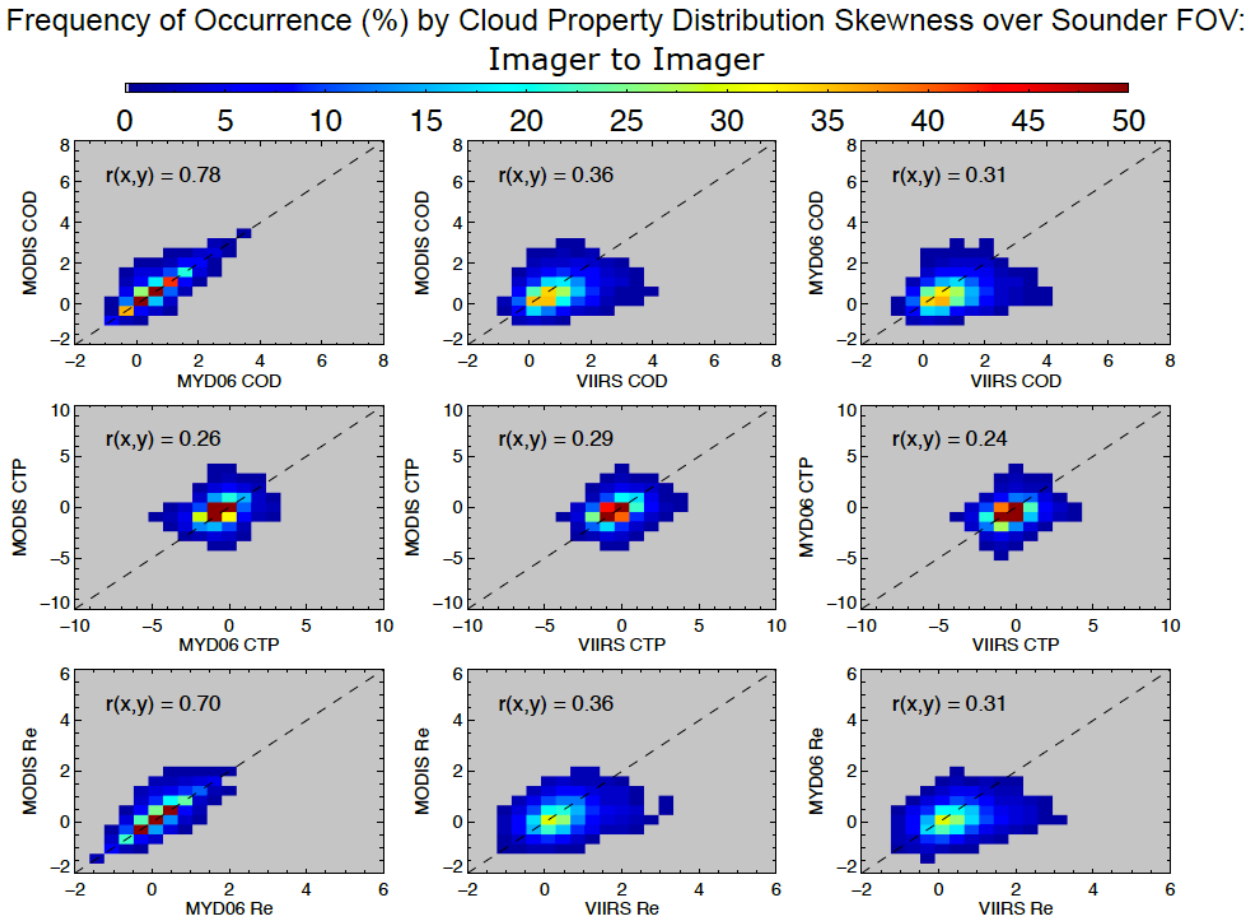

Figure 9. Similar to Figs. 8 and 7, except cloud property skewness over sounder FOV is used in the comparison. Results are shown in linear scale. Linear correlation coefficients between the variables on x- and y-axes are given in each plot.

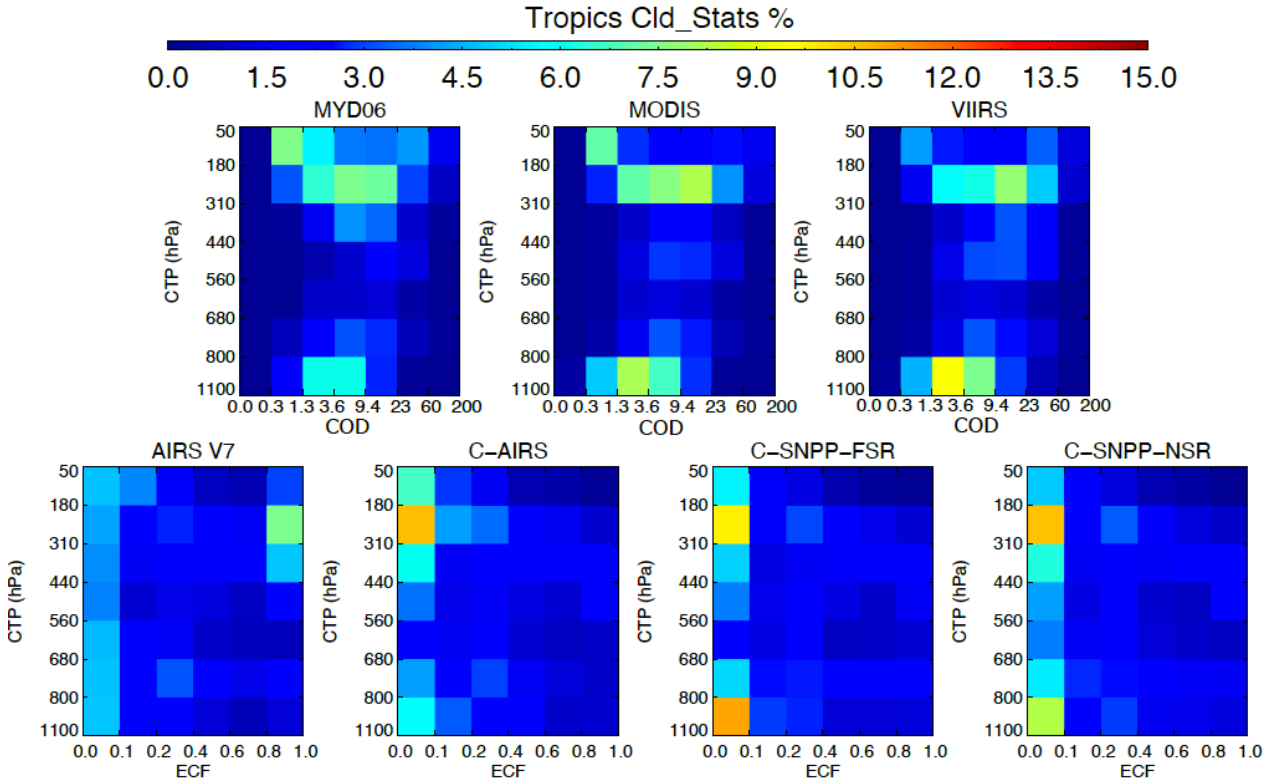

Figure 10. The 2-dimensional histograms calculated using SNOs from the focus days in the tropics (30°N~30°S). The top row shows results for MODIS and VIIRS, for which the ISCCP type of COD-CTP joint histograms are presented by summarizing the histograms over individual AIRS and CrIS FOV. Note that no averaging over sounder FOV is taken for this comparison. From left to right show results of MYD06, *Aqua*-MODIS continuity, and *SNPP*-VIIRS continuity cloud products. The bottom row shows results for AIRS and CrIS, and joint distributions are calculated on the imager effective CTP and ECF space. From left to right, data from AIRS Version 7 (AIRS

V7), CLIMCAPS-*Aqua* (C-AIRS), CLIMCAPS-*SNPP* FSR (C*SNPP*-FSR), and CLIMCAPS-*SNPP* NSR (C-*SNPP*-NSR) are used in the calculation.

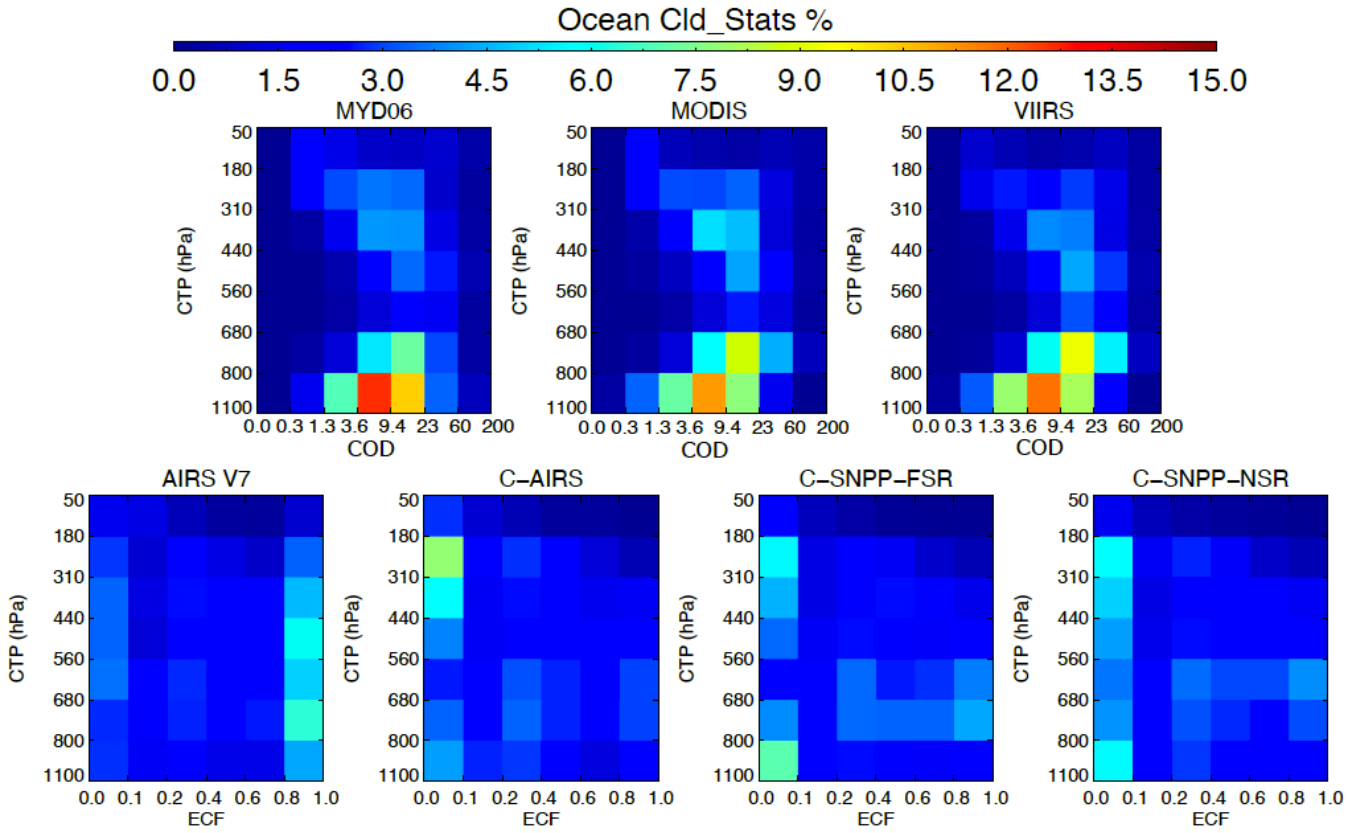

Figure 11. Similar to Fig. 10, except showing results calculated using data over 60°N~60°S ocean. Sounder land fraction < 0.1 is used to determine ocean surfaces.

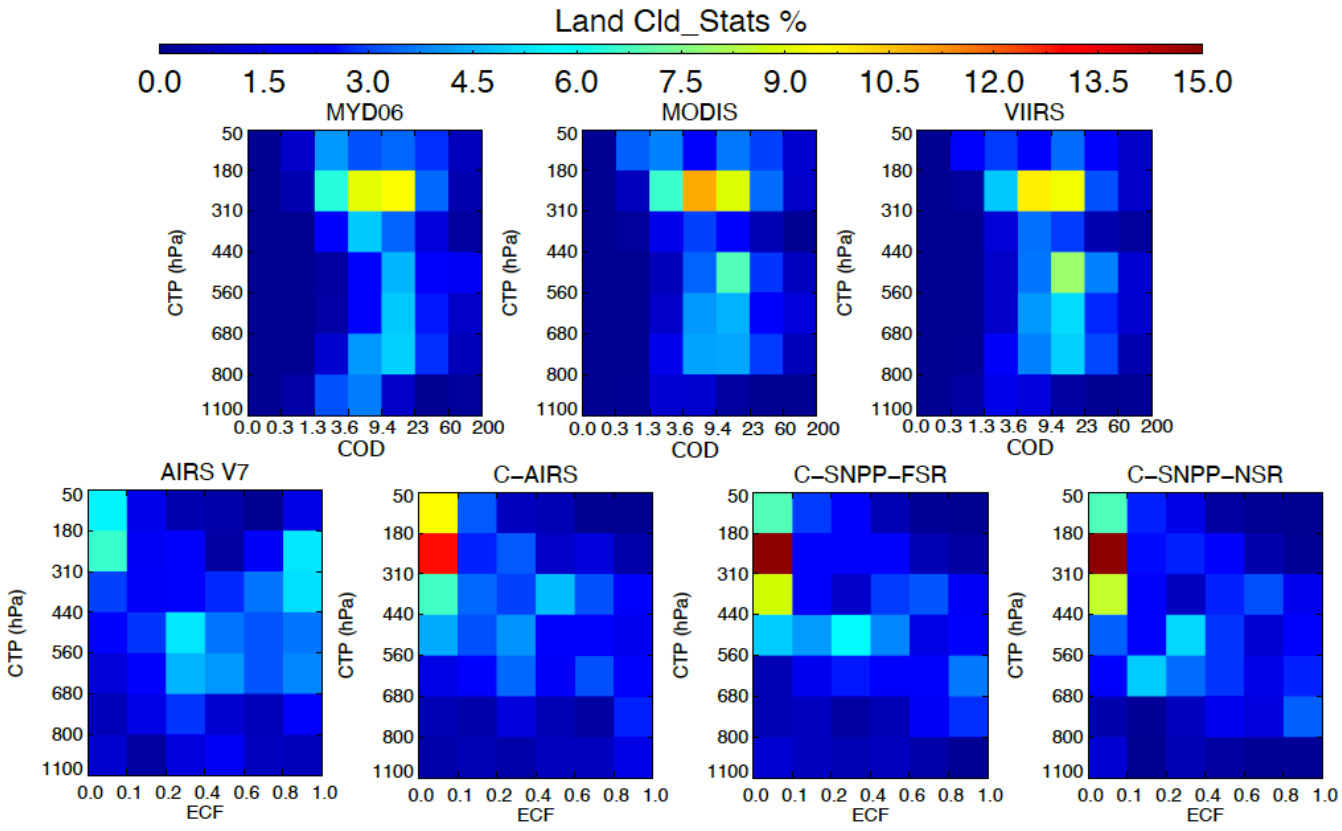

Figure 12. Similar to Figs. 11 and 10, except showing results calculated using data over 60°N~60°S land. Sounder land fraction > 0.9 is used to determine land surfaces.

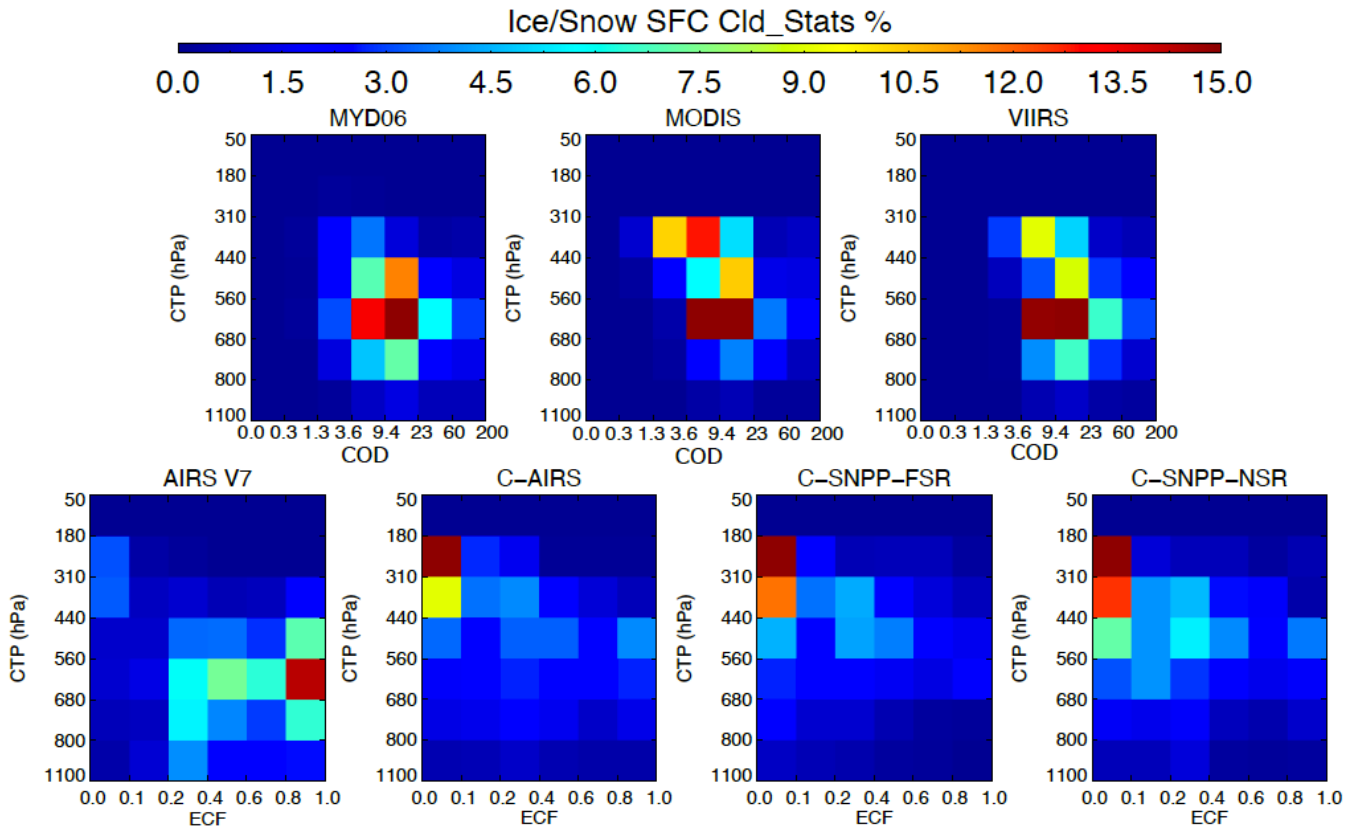

Figure 13. Similar to Fig. 10-12, except showing results calculated using data over snow and ice covered surfaces. Sounder retrieved surface classes are used to identify cases.

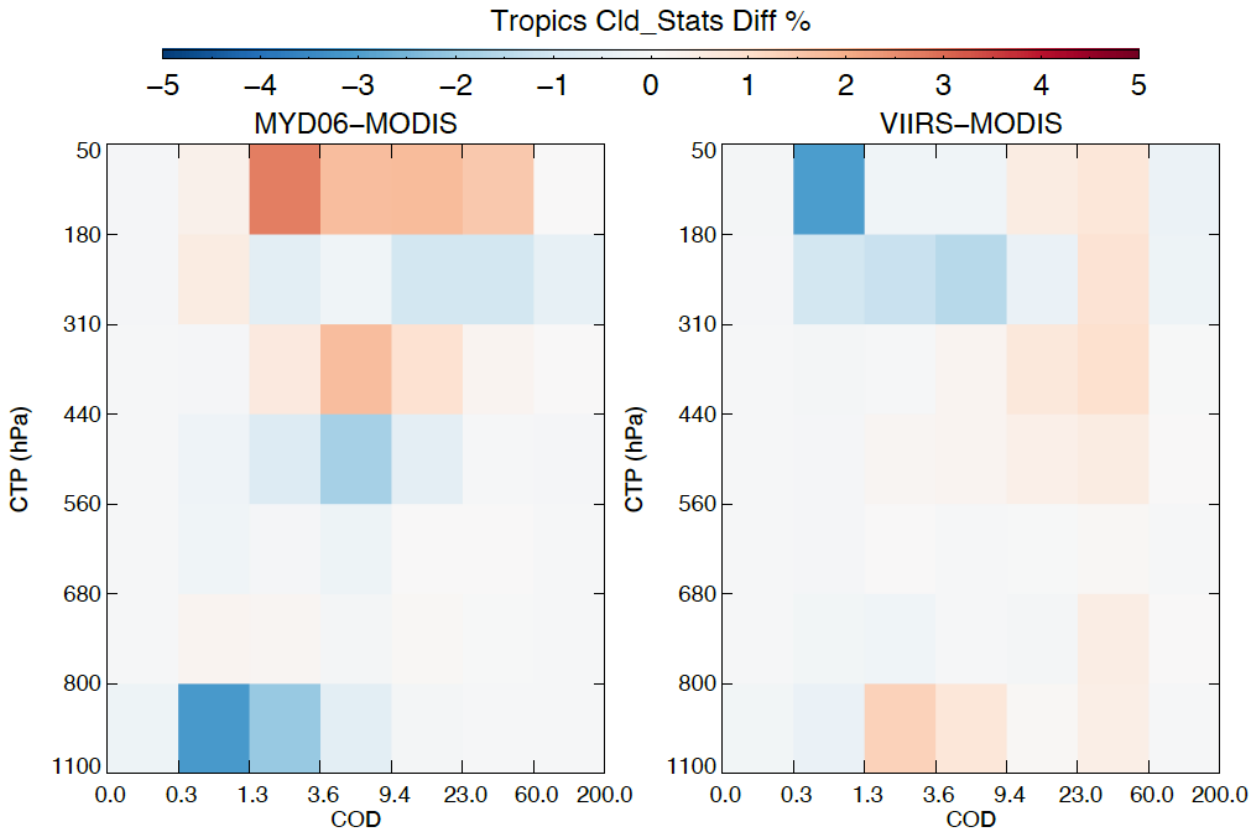

Figure 14. Differences of the imager CTP-COD cloud histograms in the tropics: between the MYD06 and *Aqua*-MODIS continuity products (left), and between the *Aqua*-MODIS and *SNPP*VIIRS continuity cloud products (right).

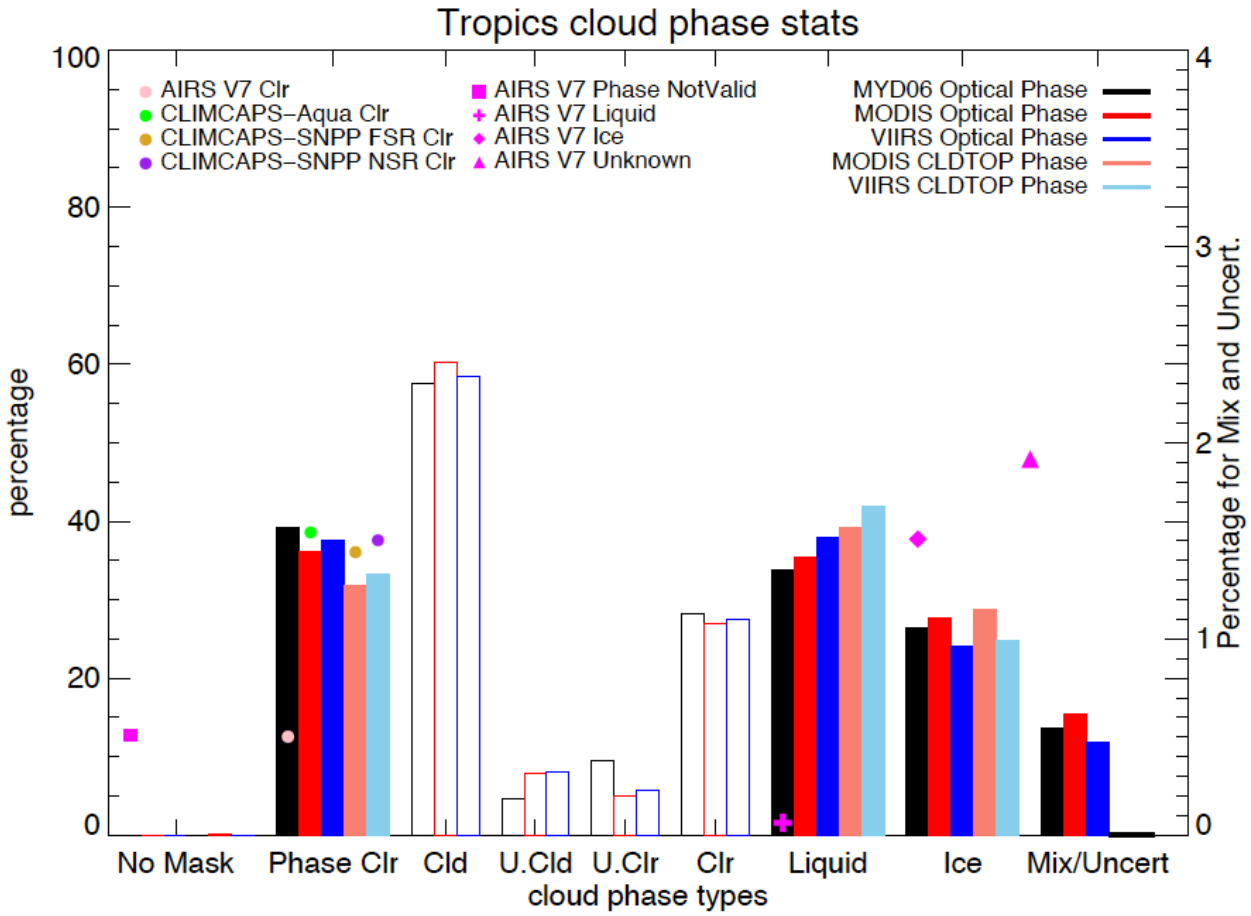

Figure 15. The histograms of cloud thermodynamic phases (solid color bars) and cloud mask (hollow color bars) in the tropics (30°N~30°S) from the imager cloud products calculated using retrievals on SNOs from the seven focus days. The frequency of clear sky detected by IR sounders using thresholds of ECF < 0.01 is also shown by colored solid circles. AIRS Version 7 cloud thermodynamic phase is shown by magenta symbols. Color of the bars corresponds with different imager cloud retrievals for cloud mask and cloud thermodynamic phase determined in the optical property retrieval (Cloud_Phase_Optical_Properties): black for MYD06, red for *Aqua* MODIS continuity products (CLDPROP_MODIS), and blue for *SNPP* VIIRS continuity products (CLDPROP_VIIRS), respectively. Cloud_Phase_Optical_Properties reports flags indicating cloud mask not determined for pixel (no mask), clear sky (Phase Clr), liquid water cloud (Liquid), ice cloud (ICE), or undetermined phase (Mix/Uncert). Cloud phases reported by Cloud_Phase_Cloud_Top_Properties in the MODIS-VIIRS continuity cloud products are also evaluated and results are shown with pink (MODIS) and light blue (VIIRS) bars, which shows flags indicating cloud free (Phase Clr), water cloud (Liquid), ice cloud (ICE), mixed phase cloud or undetermined phase (Mix/Uncert). Note that the Mix/Uncert phase category for imager products is shown with the y-axis on the right due to its much smaller frequency of occurrence. Cloud mask histograms of Not determined (No Mask), Cloudy (Cld), Uncertain (U. Cld), Probably Clear (U. Clr), and Confident Clear (Clr) are shown in the figure following this color convention but using hollow bars. For IR sounder clear sky frequency, results from AIRS V7 (pink), CLIMCAPS-AIRS

(green), CLIMCAPS-*SNPP* FSR (yellow), and CLIMCAPS-*SNPP* NSR (purple) are overlaid on top of the Phase Clr histograms for sounder-imager clear sky detection comparison.

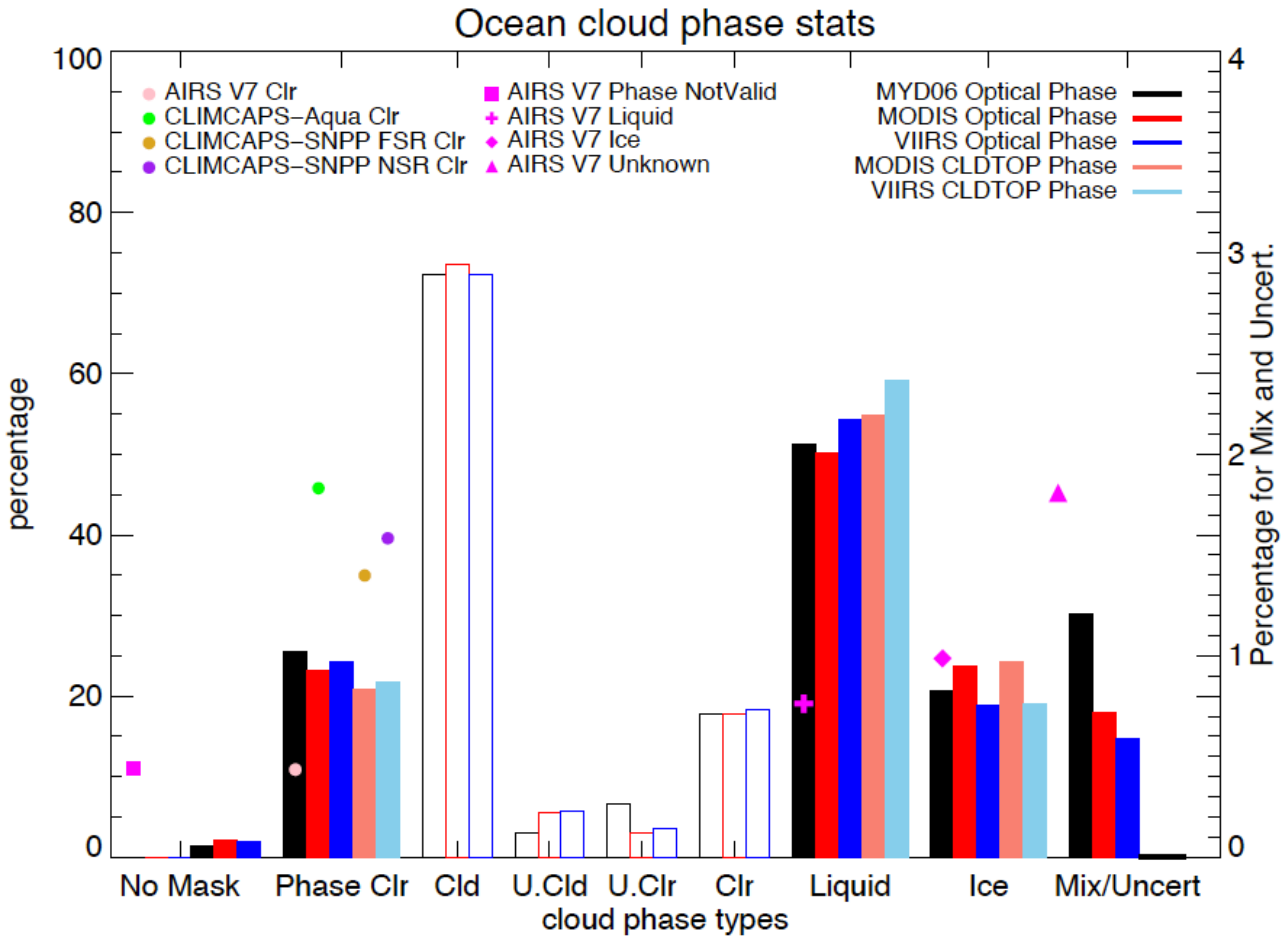

Figure 16. Similar to Fig. 15, except showing results calculated using data over 60°N~60°S ocean. Sounder land fraction < 0.1 is used to determine ocean surfaces.

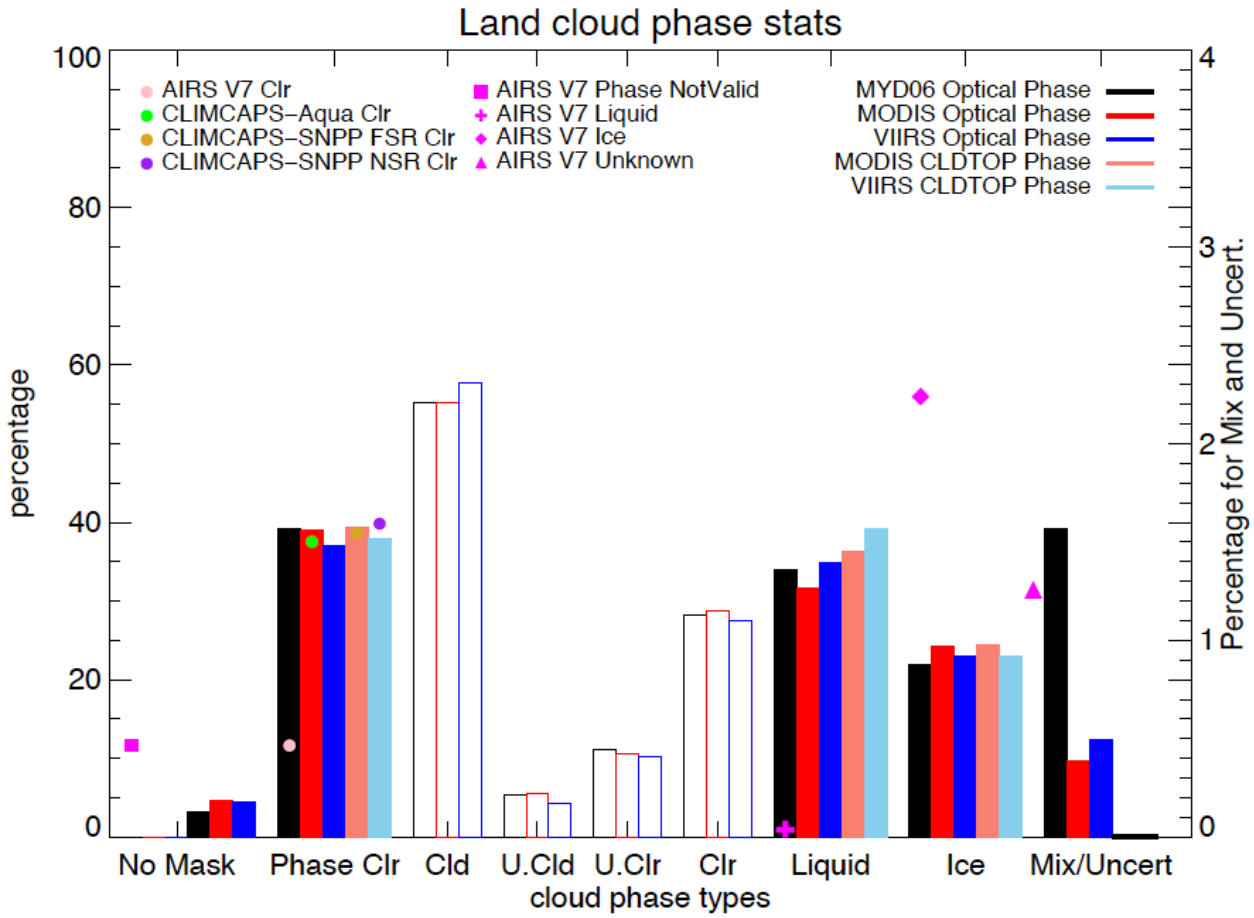

Figure 17. Similar to Figs. 16 and 15, except showing results calculated using data over 60°N~60°S land. Sounder land fraction > 0.9 is used to determine land surfaces.

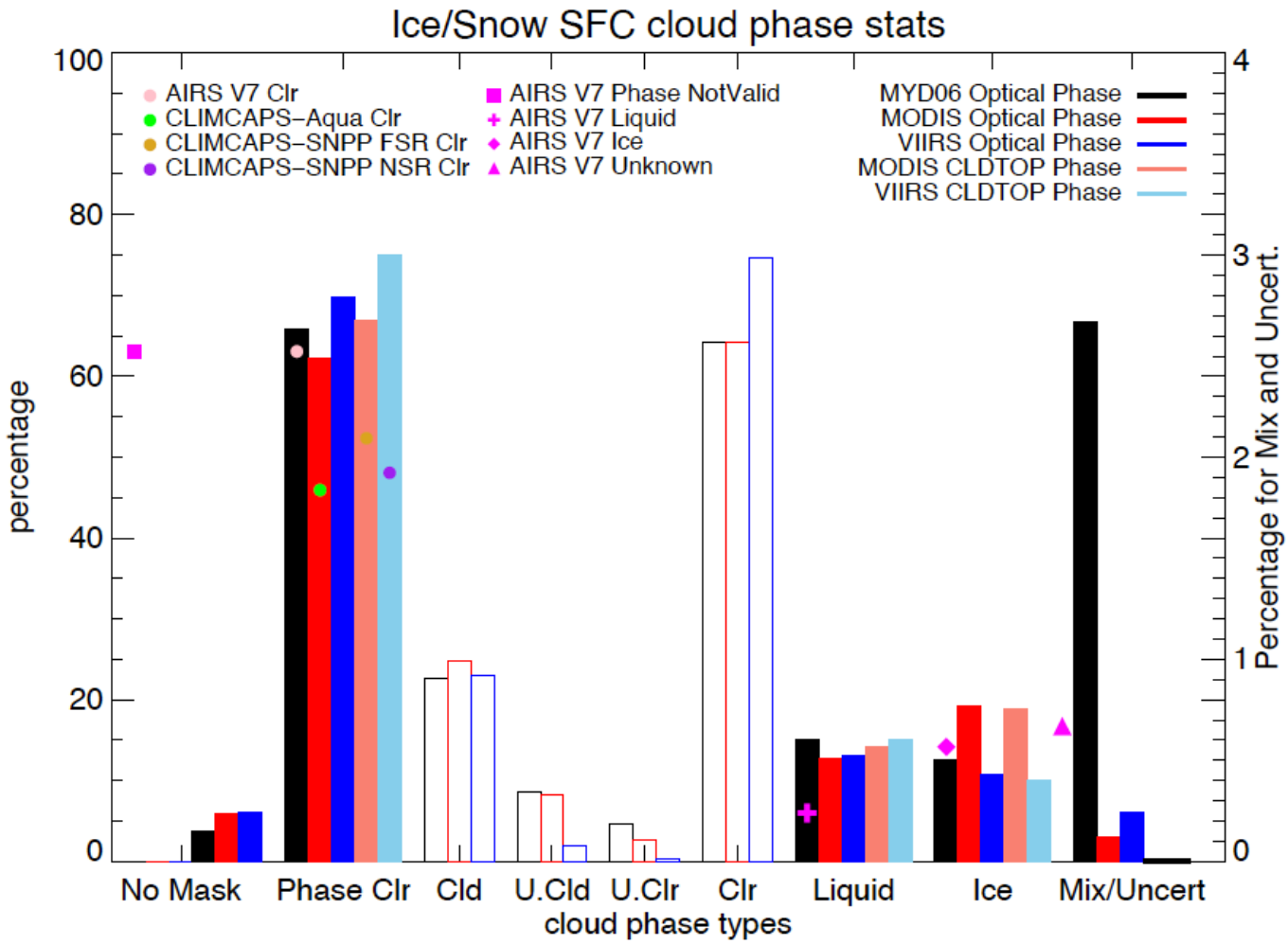

Figure 18. Similar to Figs. 15-17, except showing results calculated using data over snow and ice covered surfaces. Sounder retrieved surface classes are used to identify cases.